Universitetet i Stavanger

Faculty of Science and Technology

MASTER'S THESIS

Study program/Specialization: Petroleum Engineering/Natural Gas Technology	Spring semester, 2017 Open
Writer: **Mir, Muhammad Raza**	…… (Writer's signature)

Faculty supervisor:

Professor Rune Wiggo Time

Co-Supervisor:

Milad Khatibi (PhD candidate)

Thesis title:

Investigation of the transport mechanism of the cutting transport in drilling horizontal wells using high speed camera and PIV for analysis

Credits (ECTS): 30

Keywords: Particle transport Pressure drop Flow patterns Particle velocity Bed height 3-layer Model Comparison with literature	Pages: 65 + enclosure: 13 Stavanger, 15.06.2017

Project Title

“Investigation of the transport mechanism of the cutting transport in drilling horizontal wells using high speed camera and PIV for analysis”

(Medium-Scale Flow Loop)

Spring 2017

Department of Petroleum Engineering (IPT)

Master’s thesis

By

Mir, Muhammad Raza

Student

In cooperation, with

Prof. Rune Wiggo Time

(Professor University of Stavanger)

And additional supervisor

Milad Khatibi

(PhD Candidate)

Acknowledgement

Firstly, I would like to thank God almighty for His blessing showed on me during this period of writing master thesis work.

I would to express special thanks of gratitude to my supervisor Prof. Rune Wiggo Time for his valuable contributions, support and guidance in carrying this master thesis work. He gave me comments and feedback during whole period for better report writing and provided me ideas to tackle the problems.

In addition, I would like to thank PhD candidate Milad Khatibi for his continuous support throughout whole thesis. I would like to pay regard to Mr. Milad Khatibi (PhD) for valuable guidance, for ideas to solve problems, as well as for his zealous encouragement.

Thanks to Senior Engineer Hermonja A. Rabenjafimanantsoa, Benja, for providing me opportunity to work in laboratory and handed over keys to work in my desire schedule.

Finally, I would like to thank my family and friends for continuous support during whole period of writing master thesis.

Best Regards

Muhammad Raza Mir

Abstract

Dynamical feature of particle dunes is investigated in a horizontal drilling well. Apparently, it is quite challenging to transport the cuttings in horizontal section of the well because the cuttings tend to settle down and form a stationary bed. However, in this experimental study, the spherical particles were used to represent the cuttings in pipe flow. Different experiments were conducted in multiphase lab to have a better understanding of the fluid rheology; flow rate and pressure drop in horizontal section of the medium scale flow loop. Single phase and liquid-particle flow experiments were performed to compare different aspects. Various superficial liquid velocities applied to generate different length and height of particle dunes. In liquid-particle flow experiments, the spherical glass beads forming dune shape after 10 seconds flowing along with water in horizontal test section. The pressure drop over a length of 1.52 was measured. In addition, the images of particle dune were captured by high-speed camera during experimentations. Furthermore, the processing of the images is done by using MATLAB. The velocities of dune front and tail were computed using "MATLAB image view" to see how fast particles were moving with liquid flow. Although, the height of the bed was determined to investigate the increase or decrease in height of the dune bed while increasing superficial liquid velocities. The comparison of our study has been made with literature to see the similarities and differences so far. Furthermore, the experimental results were compared with 3-layer dynamic model as well to see if the simulations and experimental results show an agreement or observing a different phenomenon. To compare experimental and 3-layer dynamic model simulations, we used superficial liquid velocity (0.45 m/s). The 3-layer model work was done by Milad Khatibi (PhD candidate (University of Stavanger) and Johnny Petersen (IRIS Stavanger).

Table of Contents

Project Title II

Acknowledgement I

Abstract II

Table of Contents III

List of Figures V

List of Tables VIII

Nomenclature IX

1 Introduction 1

1.1 Aim of Study 1

1.2 Motivation 1

1.3 Background 2

1.3.1 Effect of Slip, annular velocity, drilling fluid rheology and flow rate on cutting transportation 2

1.3.2 Forces 3

1.3.3 Flow pattern 3

1.3.4 Effect of Particles size 4

1.3.5 Particle size distribution 5

1.3.6 Slurry Transport 5

1.3.7 Computational Fluid Dynamics 6

1.3.8 Poly-Anionic Cellulose (PAC) 7

2 Theory 9

2.1.1 Pressure loss in pipes 9

2.1.2 Particle-Image Velocimetry (PIV) 12

2.1.3 PIV arrangements in Multiphase Laboratory (University of Stavanger) 13

2.1.4 Three-layer model: 17

3 Experimental work 22
3.1 Experimental facility 23
3.2 Experimental Methodology 24
3.2.1 Summary of technique 26
3.2.2 Distribution of the particles with average value of particle diameter in mm . 27
3.3 Test Matrix: 28
4 Results and discussion 30
4.1 Experimental analysis of cutting transportation in horizontal section using Newtonian fluid (water) with different superficial liquid velocities: 31
4.1.1 Scenario 1 using superficial liquid velocity (U_{SL}=0.32 m/s) 31
4.1.2 Scenario 2 using superficial liquid velocity (U_{SL}=0.45 m/s) 37
4.1.3 Scenario 3 using superficial liquid velocity (U_{SL}=0.51 m/s) 41
4.1.4 Average Pressure gradient as function superficial liquid velocity (Three-Layer Model Vs Experiment) 44
4.1.5 Particle travelling velocity or cutting velocity as function Superficial Liquid Velocity (U_{SL}) 45
4.2 Comparison with literature 47
4.3 Comparison with three-layer model 51
4.3.1 Comparing 3-layer dynamic model with experiment using U_{SL}= 0.45 m/s ... 51
5 Conclusions 56
6 Recommendations for future work 58
7 References 59
8 Appendix 62
8.1 Attachment 1 62
8.2 Attachment 2 64

List of Figures

Figure 1: Illustration of test section to clarify PH and PL IX
Figure 2: Schematic diagram of inclined, vertical and horizontal section of the well illustration 1
Figure 3: Flow regimes with real illustration of dune (PEYSSON, Y. (2004) MODIFIED BY MYSELF 4
Figure 4: Structural formula of PAC (PELLUTEL POLY-ANIONIC-CELLULOSE, N.D.) 7
Figure 5.1: Block diagram for precise illustration of PIV technique. 14
Figure 5.2: Block diagram for calculating height, length and area of the dune bed using MATLAB application. 15
Figure 5.3: Schematic diagram of dune bed with bullet points to show the methodology of height calculation. 15
Figure 5.4: Forces acting on the particle at the upper stratum of stationary bed (Doron P and D. Barnea 1993 edited by myself) 18
Figure 5.5: Schematic illustration of three-layer model; geometry, velocities and shear stresses (Doron P and D. Barnea 1993 edited by myself) 19
Figure 6: Real view of Multiphase Lab in University of Stavanger. 22
Figure 7: Schematic diagram of medium scale flow loop of Multiphase Lab in University of Stavanger. 23
Figure 8: 3-D illustration of horizontal section of medium scale flow loop of Multiphase Lab in University of Stavanger. 24
Figure 9.0: Summery of the technique used during experimentation 26
Figure 9.1: Real illustration of the particles captured through highly accurate microscope. 27
Figure 10: Results of pressure gradients. a)- Liquid-Particle flow. b) - Single-Phase flow. c) - Combine illustration of a,b where d)- Dune height as function of length 31
Figure 11: Pipe illustration with initial condition and test section. g)-schematic diagram showing dune is @ initial condition and h)-real dune Figure moving in at initial conditions (section A). 32
Figure 12: Pipe illustration with initial condition and test section. i)-schematic diagram showing dune is at PH and j)-real dune Figure at PH (high-pressure side) (Section B). 33

Figure 13: Pipe illustration with initial condition and test section. k)-schematic diagram showing dune is in test section and l)-real dune Figure in the test section (Section C). 34
Figure 14: Pipe illustration with initial condition and test section. m)-schematic diagram showing dune is is at Low-pressure side and n)-real dune Figure is at PL (low-pressure side) (Section D). 35
Figure 15: Real illustration of dunes. e)-Initial conditions. f)-Test section 36
Figure 16: Results of pressure gradients. o) - Liquid-Particle flow. p) - Single-Phase flow. q) - Combine illustration of o,p where r)- Dune height as function of length. 37
Figure 17: Pipe illustration with initial condition and test section. u)-schematic diagram showing dune is @ initial condition and v)-real dune Figure moving in at initial conditions (section A). 38
Figure 18: Pipe illustration with initial condition and test section. w)-schematic diagram showing dune is at PH and x)-real dune Figure at PH (high-pressure side) (Section B). 38
Figure 19: Pipe illustration with initial condition and test section. y)-schematic diagram showing dune is in test section and z)-real dune Figure in the test section (Section C). 39
Figure 20: Pipe illustration with initial condition and test section. 20.1)-schematic diagram showing dune is at Low-pressure side and 20.2)-real dune Figure is at PL (low-pressure side) (Section D). 39
Figure 21: Real illustration of dunes. s)-Initial conditions. t)-Test section. 40
Figure 22: Results of pressure gradient as function of time with average value flow reaching to single phase 41
Figure 23: Height of the dune as function of length. 42
Figure 24: Real illustration of dunes. 24.1)-Initial conditions. 24.2)-Test section. 43
Figure 25: Averaged pressure gradient as function of superficial liquid velocity 44
Figure 26: Dune bed illustration at lower Superficial Liquid Velocity 45
Figure 27: Dune bed illustration at higher Superficial Liquid Velocity 45
Figure 28: Liquid velocity as function of dune bed velocity 46
Figure 29: Schematic illustration of dune bed with front and tail velocity points 46
Figure 30: Schematic illustration with measurements with initial and boundary conditions (Medium scale flow loop, horizontal section). 51
Figure 31: Comparison of three-layer dynamic model simulation with experiment using USL= 0.45 m/s 52
Figure 32: Schematic illustration of dune bed in case of 3-layer model and experiment at initial condition and at PH. 54

Figure 33: Schematic illustration of dune bed in case of 3-layer model and experiment at initial condition and at PL. 55

Figure 34: Real illustration of equipments used in Multiphase Laboratory University of Stavanger..... 63

List of Tables

Table 1.0: Measurement of particle diameter used in experiment of medium scale flow loop in Multiphase Lab University of Stavanger…… 28

Table 1.1: Specification of the experiment of medium scale flow loop in Multiphase Lab University of Stavanger…… 36

Table 2: Results of four experiments with different parameters…… 37

Table 3: Detail illustration of each author with different input parameters…… 56

Table 4: Detail illustration of each author with their title…..... 57

Nomenclature

Abbreviations with subscripts:

U_{SL}	Superficial liquid velocity
PH	High-pressure side of test section
PL	Low-pressure side of test section

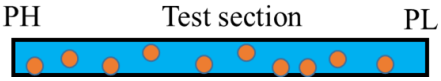

Figure 1: Illustration of test section to clarify PH and PL

f_F	Fanning friction factor
PAC	Poly-Anionic Cellulose
PIV	Particle image velocimetry
V_{Front}	Velocity of the dune front (mm/s)
V_{Tail}	Velocity of the dune tail (mm/s)
ECD	Equivalent circulating density
Re_{cr}	Critical Reynold number
CFD	Computational Fluid Dynamics
LED	Light Emitting Diode
FPS	Frame per second
F_D	Driving force (N)
ρ_L	Density of carrier liquid $\left(\frac{Kg}{m^3}\right)$
U_{bc}	Critical bed velocity (m/s)
C_D	Drag coefficient of particle
A_P	Area on which drag force act on it (m^2)
d_p	Particle diameter (m)
U_h	Heterogeneous upper layer axial velocity (m/s)
C_h	"C" denotes volumetric concentration of solid particles and subscript "h" denotes heterogeneous upper layer
A_h	Pipe cross sectional area and subscript "h" denotes heterogeneous upper layer And subscript "mb" denotes moving bed in above equations. (m^2)

U_s	Slurry superficial mean velocity (m/s)
C_s	Slurry input concentration
A_h	Cross sectional area occupied by dispersed layer (m^2)
A_{mb}	Cross sectional area occupied by moving layer (m^2)
$\frac{dp}{dx}$	Pressure drop (Pa/m)
τ_h	Shear stress at the pipe circumference
τ_{mb}	Interfacial shear stress
S_h	Interface of disperse layer
S_{mb}	Interface of moving layer
ρ_h	Effective density of upper layer
f_{hmb}	Friction coefficient at pipe wall and moving layer
U_{mb}	Axial velocity of moving layer
ρ_s	Density of solid particles (kg/m^3)
ρ_L	Liquid density (kg/m^3)
Re	Reynold number
V	Flow velocity [m/s]
D	Inner diameter of the pipe [m]
v	Kinematic viscosity [m^2/s]
A_rel	Relative area of the dune bed (dimensionless)

Greek letters:

$\emptyset$	Angle
Π	Pi (3.1416 constant value)
ΔP	Differential pressure
τ_w	Wall shear stress (Pascal)
ρ	Density [kg/m^3]
$\bar{u}$	Average flow velocity [m/s]
$\propto_h$	0.046 for turbulent flow
β_h	0.02 for turbulent flow
$\propto_h$	16 for laminar flow
β_h	1 for laminar flow

Basic definitions:

Bernoulli Effect: In fluid dynamics, the Bernoulli effect states that if the increase in fluid speed happened simultaneously while decreasing the pressure and vice versa.

ECD (Equivalent circulating density): Effective density homogenize the current mud density and annular pressure drop. However, it is very crucial parameters in drilling because it can cause severe losses due to high-pressure loss in annulas.

1 Introduction

In this chapter, the purpose of this study and relevant background unfolded precisely. However, background included brief introduction of cutting transportation, factors effecting cutting transportation and most importantly flow pattern and effect of flow pattern while increasing or decreasing U_{SL} (superficial liquid velocity).

1.1 Aim of Study

The purpose of this study was to investigate the cutting transport behavior in horizontal section of the pipe. For this, different experiments were conducted for better understanding of the cutting transport behavior. Firstly, the aim was to compute the pressure gradient using LabVIEW software (already installed in computer) with different superficial liquid velocities. Secondly, to find out the dune front and tail velocities to observe how fast particles are moving along with water using MATLAB application. The height of the bed was also very significant parameter to be considered during this tenure. In addition, bed height was determined to see how height and length of the bed was changing with varying superficial liquid velocity.

1.2 Motivation

Many researchers have conducted the different experiments and observations to solve the mystery of transport behavior and complexity of transporting cuttings from horizontal section of the well. Cuttings tend to settle down in horizontal section and become harder to transport through the annulus compare to inclined and vertical wells where cutting can easily be transported as it can be seen in Figure A. The challenge of cutting transportation is in era now. As motivation, we took this challenge to try to solve the complex mystery of transporting cuttings in horizontal wells by conducting different experiments in Multiphase Phase Lab university of Stavanger.

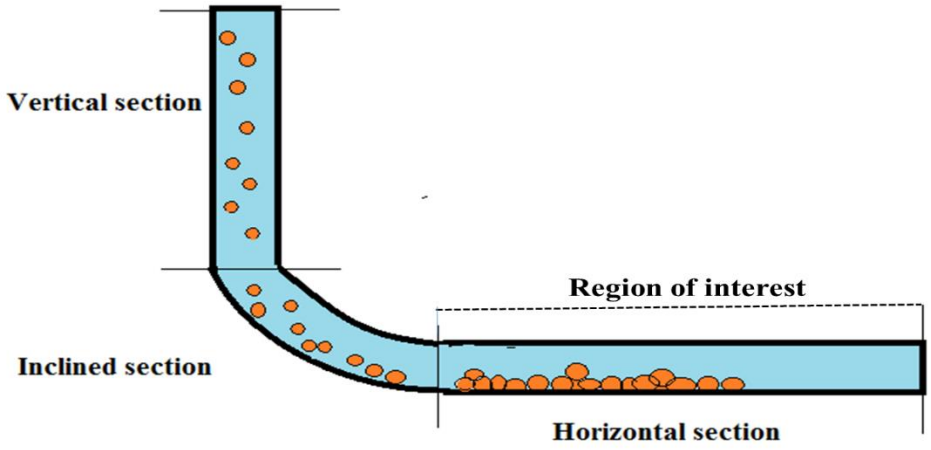

Figure 2: Schematic diagram of inclined, vertical and horizontal section of the well illustration.

1.3 Background

When an oil well is about to be drilled, it is very significant to remove and transport the cuttings from the reservoir to wellhead. Pumping the fluid (drilling fluid) from the center of the drill pipe can help to transport the cuttings through annular gap between drill hole and drill pipe. However, the fluid is non-Newtonian and highly viscous and occupying the gel strength. The flow from bottom and up to the annulus might be laminar or turbulent varying on situation (Woo, N.S, et al 2011).

Cuttings transportation is a method, which can be considered throughout entire drilling procedures to avoid cuttings interruption and to limit the negative effects of cuttings. Poor hole cleaning can lead to several problems such as bit wear, slow drilling rate, Increased ECD (Equivalent circulating density) which can lead to formation fractures, high torque, drag and it can lead to stuck pipe situation which is worst.

Cuttings transport mechanism is controlled by different variables for instance, well inclination, angle, hole and drill pipe diameter, drill pipe rotation speed, drill pipe eccentricity, rate of penetration, cutting characteristics, fluid velocity, flow, regime, mud type and non-Newtonian mud rheology (Egenti, 2014).

Three major factors need to be fulfilled to have efficient bore-hole cleaning:

1. Washing at Mud-rock interface.
2. Cross flow controlling and minimizing the regrinding of the cuttings
3. Fast lifting of the cuttings around bit face (Bizanti,M.S, 1983).

1.3.1 Effect of Slip, annular velocity, drilling fluid rheology and flow rate on cutting transportation

Slip velocity correlation has been formulated for the past fifty years and it is recommended to use proper annular velocity to avoid the slippage of the cuttings around drill collar and drill bit. However, slippage can cause regrinding of the cuttings and this is the wastage of the limited power that we must operate the drill bit. An average annular velocity of 80 to 120 ft. /min is reasonable and observed in oil and gas industry to satisfy proper hole cleaning (Bizanti et al, 2003). Drilling fluid rheology and flow rate are two main parameters which play vital a role in cutting transportation. The properties of drilling fluid that affect hole cleaning are mud weight and drilling fluid viscosity. The basic purpose of mud density is to prevent the interference of formation fluid. Increasing the mud density will cause cuttings suspension but on another hand, high mud density lower the rate of penetration, which will increase drilling cost. Therefore, mud

weight should not be increased for whole cleaning. Furthermore, it is predicted that in all cases the most effective parameter in developing a cuttings bed is flow rate. However, increase in flow rate will prevent the cutting bed development because for a higher flow rate, higher shear stress is exerted onto the cutting bed, which prevent the bed formation. When flow is turbulent, the cuttings are carried out effectively. As the flow rate increases then the accumulation of cuttings on lower side of the well will decreases until value where no cuttings accumulation occurs (Mohammadsalehi,M., et al, 2011).

1.3.2 Forces

Cuttings transport mechanism can be illustrated by considering the forces that acts on single cutting when the cutting settles on lower side of the wellbore. The forces are divided into two groups:

1. Depositional forces
2. Transport forces

Depositional forces are divided into two further forces namely gravitation and frictional forces. Due to gravitational force, the cuttings settle down and eventually form bed. Frictional force is force that act against cutting movements and transport forces are divided into two forces namely lift and drag forces. The lift forces lift the cuttings and transport them with flow stream. The drag forces roll the cuttings to move them forward direction (Egenti, 2014).

1.3.3 Flow pattern

The flow regime of cuttings will have different flow patterns. In heterogeneous flow pattern, the lift forces are much stronger then gravitational forces that is why cuttings are lifted and transported in suspension form. Heterogeneous suspension occurs at high fluid velocity. In homogeneous suspension flow pattern, cuttings are transported in suspension form but uniformly distributed over annular space. In saltation flow pattern, particles are transported in suspension form. However, they are directed to low side of the annulus and are transported by jumping forward or saltating on the surface of the low side of the wall. If suspension dominated, then it is called suspension/saltation and if saltation is dominated, then it is said as saltation/suspension flow pattern. Separated cuttings bed form on the lower side of the annulus. In this type of flow pattern, cuttings on surface of the bed move forward while cuttings inside the bed remain stationary. This flow pattern formed when lift forces and drag forces combines. This flow pattern arises due to low fluid viscosity and flow is turbulent. Cuttings are transported by rolling and sliding effect. In continuous moving bed flow pattern, a thin layer of moving bed formed on lower side of the wellbore and it is only drag force that drag the cuttings to forward direction.

This kind of flow pattern occurred on high fluid viscosity and flow is laminar. If the cuttings are transported in suspension but in clusters form, all cuttings in each cluster will be transported with same velocity. This is called as clusters cutting bed. In stationary bed, rolling or sliding forces transport the cuttings while the cuttings inside the bed remains stationary (Egenti, 2014). Figure 3 indicates the flow pattern, which is modified in this thesis.

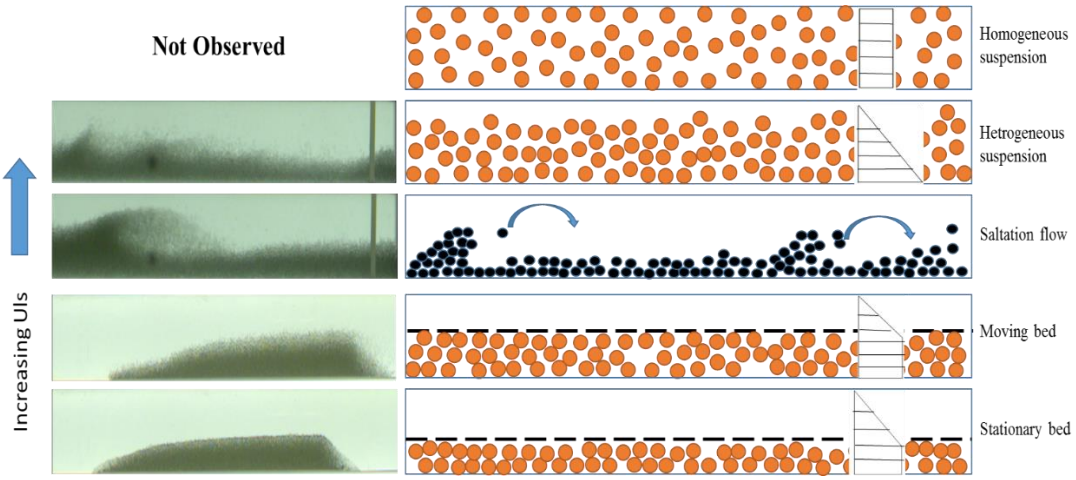

Figure 3: Flow regimes with real illustration of dune (PEYSSON, Y. (2004) MODIFIED BY MYSELF.

The flow regime has direct effect on cutting transport. However, flow can be either laminar or turbulent. The flow regime is depending on fluid velocity, size and shape of annulus, fluid density and viscosity. The flow regime between laminar and turbulent is transitional zone; in this region, fluid will have both laminar and turbulent characteristics. During the drill pipe rotation, turbulent flow can be formed. However, when the fluid velocity is low or viscosity is high the flow is laminar. On the contrary, when flow velocity is high and viscosity is low the turbulent region is formed (Egenti, 2014).

Goharzadeh et al have made investigation of solid particle transport in horizontal pipeline and they found that the physical mechanism of sand transportation was internment (discontinuous) and the elongated bubble flow and slug body highly effects the transport of sand particles in horizontal pipeline (Goharzadeh et al,2013).

1.3.4 Effect of Particles size

The density, size and surface appearance of the particles have major effect on the dynamic behavior in flowing media. Different studies have been conducted using different particles sizes and particles concentration to investigate the effect of particle transport. However, the terminal

velocity, drag force, buoyant corrected gravity force and shear force between cutting is highly influenced by properties of cuttings and circulated fluid (Walker et al, 2000). Spherical glass particles with higher density than water are preferred to avoid the sharp edges on cutting (Shook et al, 1991).

1.3.5 Particle size distribution

The particle size can be a very significant parameter in the flow of dispersed two-phase mixture and that is why it is very important to know more about statistical parameters related to particle size distribution. For spherical particles, diameter is considerable for measurement but for non-spherical particles, an equivalent diameter is confirmed to express the size of the particle.

Crowe et al, 2011 explained in their book that particle size distribution can be expressed by two terms named as:

1. Mono-disperse
2. Poly-disperse

In mono-disperse type distribution the particles are nearly close to single size. More precisely we can say that in mono-disperse type particle distribution the standard deviation is less than 20% than mean particle size. In poly-disperse type distribution the wide range of particles sizes are recommended. Liquid solid flows comprises of flow in which solid particles are being transported by liquid and called as slurry flows (Crowe et al, 2011).

1.3.6 Slurry Transport

Slurries are categorized as homogenous, heterogeneous, moving bed or stationary bed. Homogeneous slurries comprise of small particles. Homogeneous slurries contain small particles sustained in suspension form by the turbulence of carrier fluid whereas heterogeneous slurries consist of coarse particles that gravitate to settle bottom of the pipe. The velocity at which particles settle out known as deposition velocity, which is analogous to saltation velocity in pneumatic transport. Undoubtedly, no slurry will be entirely homogenous. However, the slurry is homogenous is the discrepancy between the concentration of the particles is less than 20%.

The moving bed regime takes place when the particles tend to settle on the bottom of the pipe and move beside the bed due to which flow rate is reduced because the bed is moving very slowly compared with fluid moving above bed. When it fills the channel and no further motion is possible, then stationary bed will start appearing in pipe flow (Crowe et al, 2011).

The fluid mechanics of the liquid solid flow is quite complicated because of the particle-particle and liquid-particle interaction.

1.3.6.1 Interactions

Particle-fluid is more likely concerned with exchange of the properties between phases and is accountable for coupling in disperse phase flow. Particle-particle interaction regulates the movement of particles in closely packed particle flow. Particle-particle interaction is not significant in dilute gas particle flow. As the particle concentration becomes higher, then the particles start colliding with each other resulting in loss of kinetic energy due to particle collision could be experienced and cannot be ignored. In multiphase flow, two spectacles are discovered that are collision and contact (Crowe et al, 2011).

Crowe et al, 2011 explained that if two spheres (spherical particles) are approaching each other in fluid and the distance between two spheres becomes smaller on other hand the fluid pressure between two spheres becomes larger than resultant force will restrict the contact of the particles.

Particle-wall interaction can be categorized by two type's namely hydrodynamic interaction due to proximity of the wall and mechanical interaction caused by contact with the wall. The Saffman lift force due to velocity gradient is one of the example of hydrodynamic interaction. However hydrodynamic interaction of this type prevents the particles for making wall contact but if the collision takes places in times much less, than hydrodynamic relaxation time, then hydrodynamic interaction could be neglected. The mechanical action associated with particle-wall interaction depends on inertia of the particle. When massive or dense particle collide with the wall it bounces back but loose lot of kinetic energy due to friction and inelasticity effects. When the smaller particles ted to approach the wall, molecular forces become dominant than inertial forces due which particles get capture by wall due to cohesive forces and cohesive forces is recognized as van der Waals forces (Crowe, et al, 2011).

1.3.7 Computational Fluid Dynamics

The computational fluid is a successful tool in various fields of fluid flow. Other applications of CFD including design and manufacturing of drill bits and bit hydraulics. Many researchers simulated drilling conditions to conceptualize the velocity and pressure gradients for different well bore and bit geometry. However, the CFD software resolve the Navier-Stroke fluid dynamic equation using numerical methodology. The desired geometry is expressed by mesh volumes.

The mixed mesh volumes can be used to create the complex geometries whereas the grid refinement helps to forecast the flow fields with large gradients (Bilgesu, H. I. et al 2002, January 1).

The CFD use in the simulation of multiphase flow has been applied mostly for small diameter pipe applications. Some research studies have shown that the range of velocities applied is limited to lower superficial velocities. As the result of deformability of interface between two phases, different flow pattern can be formed in pipe. Therefore, any numerical methodology caused by undesirable discretization scheme can lead to false and incorrect CFD predictions (Parsi, M. et al, 2015, September 4).

1.3.8 Poly-Anionic Cellulose (PAC)

(Khatibi. et al, 2016) explained very well in their journal article about PAC. Poly-Anionic Cellulose (PAC) is semi natural anionic sodium Carboxyl-Methyl Cellulose with high degree of substitution, high uniformity and high quality. Because of these qualities, it is sometime regarded as Premium quality additive. In drilling PAC is likely to be used with wide range of total solid content, salinity and ph. However small concentration of PAC provide effective reduction in filtration rate and fine rheological stabilization (Khatibi.et al , 2016).

The molecular formula of the PAC is $[C_6H_7O_2(OH)_2OCH_2COONa]_n$ and structural formula in Figure 4:

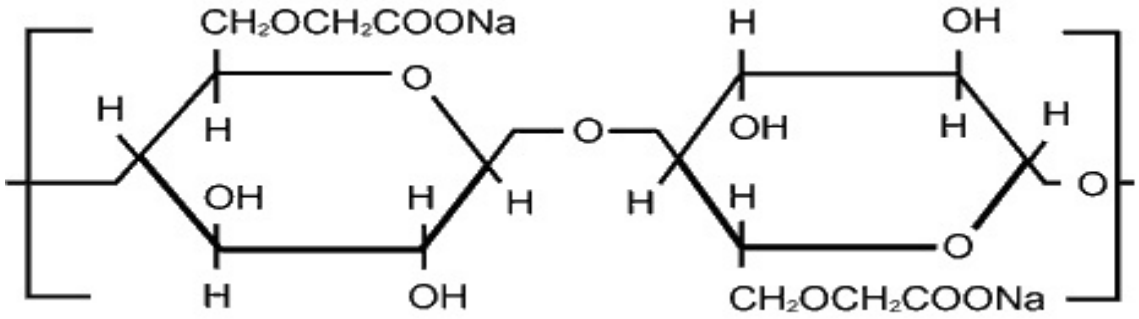

Figure 4: Structural formula of PAC (PELLUTEL POLY-ANIONIC-CELLULOSE, N.D.)

1.3.8.1 PAC dissolution technique

PAC mixture preparation was organized based on Kelco CMC manual. The pre-determined amount of PAC powder is precisely poured in to deionized water in a mixing facility so all individual particles become entirely wetted and it is very significant to keep the rotation speed of the agitator high enough to maintain low viscosity. `However, the rotation speed was 3000 rpm and after some time it decreased to 2000 rpm for 30 minutes. Solution is placed at 21°C

temperature for 48 hours and during this procedure small entrained air bubbles will separate out eventually (Khatibi. et al, 2016)

1.3.8.2 Applications of PAC-R solution

PAC helps to form the tough, thin filter cake to avoid the impact of differential sticking. PAC is very useful to viscosifying all type of water to enhance the solid carrying ability to facilitate the proper hole cleaning. To form the viscosity, range from 1.0 to 4.0 lb. /bbl. (3.0 to 12.0 kg/m^3) recommended concentration (Company, 2004).

2 Theory

2.1.1 Pressure loss in pipes

To find out the pressure loss or flow rate, friction factor is required between fluid and the pipe. However, pressure drop without any diameter change occur due to friction between fluid and the pipe. Friction factor is used to determine pressure loss in the pipe. Although there are two types of friction factors namely Darcy and fanning type friction factors. The Darcy friction factor is also named as Darcy-Weisbach friction factor or Moody friction factor. The Darcy friction factor is 4 times that of fanning friction factor according to the article (Neutrium, 2012):

$$f = 4\, f_F \qquad \text{(eq 1)}$$

f_F = Fanning friction factor

2.1.1.1 Darcy-Weisbach friction factor

The pressure loss in the pipe can be calculated using Darcy-Weisbach friction factor, which is given by eq 2:

$$\Delta P = f\, \frac{L}{D}\, \frac{\rho V^2}{2} \qquad \text{(eq 2)}$$

Where

ΔP= Pressure loss in the pipe

f = Darcy friction factor

L = Length of the pipe

D = Inner diameter of the pipe

ρ = Density of the fluid

V^2 = Flow velocity

(Kiijavi, 2011)

(Su, Ze et al, 1993) described very well in their article about how we can calculate the friction factor using pressure drop equation, which we already mentioned above eq2. Apart from this method they explained that we can calculate the friction factor using velocity profile near the wall of the pipe and velocity distribution law used to find out friction velocity (u^*) from which we can calculate wall shear stress and finally friction factor can be determined using following formula:

$$f_M = \frac{8\,\tau_W}{\rho\,\bar{u}^2} \qquad \text{(eq 3)}$$

In which

f_M = Moody friction factor

τ_w = Wall shear stress

$\rho = Density$ [kg/m^3]

$\bar{u}$ = Average flow velocity [m/s]

However, u^* in universal velocity distribution law is known as friction velocity. The relation for computing friction velocity is given below:

$$u^* = \sqrt{\frac{\tau_w}{\rho}} \qquad \text{(eq 4)}$$

In which u^* is friction velocity where τ_w is wall shear stress which associate to pressure drop in pipe flow as

$$\tau_w = \frac{D}{4}\frac{d_p}{d_x} \text{ (eq 5)}$$

The wall shear stress can be computed by calculating pressure drop in the pipe flow test and finally friction velocity can be measured by using wall shear stress as mentioned above equation (Su, Ze et al, 1993).

2.1.1.2 Colebrook

The Colebrook equation is used to solve the Darcy friction factor. The equation is given below:

$$\frac{1}{\sqrt{f}} = -2.0 \log\left(\frac{e/_D}{3.7} + \frac{2.51}{Re\sqrt{f}}\right) \qquad \text{(eq 6)}$$

in which

f = Darcy friction factor

e = roughness of the pipe

D = inner diameter of the pipe (m)

Re = Reynold number

However, the ratio e/D is called relative rough.

2.1.1.3 Reynold number

Reynold number can be determined using following relation:

$$Re = \frac{V\,D}{v} \qquad \text{(eq 7)}$$

In which

Re = Reynold number

V = flow velocity [m/s]

D = inner diameter of the pipe [m]

v = kinematic viscosity [m^2/s]

The Reynold number clarify whether the flow is laminar or flow is turbulent. If the Reynold number is smaller than critical Reynold number ($Re_{cr)}$ then flow will be laminar. The laminar flow will eventually follow the transition region. When the Reynold number reaches to the certain value then flow will switch from transitional to turbulent. The critical value for Reynold number for pipe flow is around 2300 and transition region stopped at around Reynold number 4000 (Kiijavi, 2011).

2.1.1.4 Blasius

Blasius model can be used to solve the Darcy friction factor and it is quite simple because it has no pipe roughness term in it. It is only applicable for smooth pipe but sometimes it can be used in rough pipe case because it's very simple to solve and find friction factor much easier.

$$f = \frac{0.316}{Re^{0.25}} \qquad \text{(eq 8)}$$

In which

f = Darcy friction factor

Re = Reynold number

2.1.1.5 Haaland

Haaland model is also used to solve the Darcy friction factor and correlation and is given below:

$$\frac{1}{\sqrt{f}} = -1.8\log\left[\left(\frac{e/D}{3.7}\right)^{1.11} + \frac{6.9}{Re}\right] \qquad \text{(eq 9)}$$

In which

f = Darcy friction factor

e = roughness of the pipe

D = inner diameter of the pipe

Re = Reynold number

2.1.2 Particle-Image Velocimetry (PIV)

Particles Image Velocimetry is technique to measure the instantaneous fields of velocity by measuring the displacements of the number of fine particles that are precisely following the motion of flowing fluid.

$$v = \frac{\Delta x}{\Delta t} \qquad \text{(eq 10)}$$

The test set up for this PIV framework comprises of many sub networks. However, it is necessary to put the tracer particles together with the flow. These particles must be enlightened for plane about stream no less than double inside short interim about the long haul. The dispersed light by particles is recorded using single frame or segment of the frame. However, one can analyze the PIV recordings to resolve the particle image displacement between light pulses (Raffel, M. et al, 2013)

The particles scattering, generating and dispersing properties are very sensitive and it needs to be considered carefully while performing Particle Image Velocimetry (PIV). Other proprieties including ability to scatter to generate low noise image and ability to point out some points in space to sort out the flow field spatially and finally its ability to follow the motion of the fluid precisely with interrupting the flow of fluid.

Although the seeding particles are introduced in flow of fluid that are small to follow the fluid motion but must be large to scatter the bright light energy enough to form bright image normally few micrometers in gaseous fluid and some tens of micrometers ion liquid.

Particles are very advantageous as they are the markers of the fluid as they produce very nice optical image than dyed fluid as they are very small (0.1-50μm) particle do not diffuse.

Since the particles are very small so it is quite possible to mark the fluid at any point (10^3 - 10^6) without overcharging the flow. However, it is very reasonable to use the spherical particles because the images are not dependent of particles rotation.

The drawback of the particle markers is that they must slip enough to generate the drag force required to follow the fluid motion. The slip velocity can be maintain acceptably small by proper seeding of the particles.

Particles do takes place in all fluid unless it is properly clean. In PIV results are attained by using artificial seeding particles (Adrian, Ronald J., and Jerry Westerweel. 2011).

2.1.3 PIV arrangements in Multiphase Laboratory (University of Stavanger)

In PIV arrangements, LED was used to spread light into the test section to see particle bed more precisely (A uniform white light LED panel giving background illustration) and high-speed cameras were utilized to capture the movement of the dune in to the test section. A Basler A800-510um color (500 fps (frame per second) with full resolution 800×600 camera) used in these experiments. The particle behavior can be viewed by using different flow rates controlled by frequency converter in the laboratory. From the pictures, we processed the data into the MATLAB software application.

2.1.3.1 Front and tail velocities of the dune bed

Initially, the images of the dune bed were captured using high speed cameras. In addition, the dune bed images were processed in the MATALB software application where the desired images of the dune bed were inserted for further processing. Primarily, the front velocity of the dune was computed to see how fast particles were moving on the front side of the dune and this is done by inserting the image and placing the pointer just onto the desired point of the dune bed. An X and Y values appeared just below the screen. Two different frames of images were utilized to see the difference in the particle movement with passage of time. However, the values were in the pixel's format and theses values were converted to centimeters (cm). Eventually, we managed to compute velocity because we had the displacement between two frames and time interval between these frames as well. Figure 5 is clear illustration of front velocity measurement. Although, an average of minimum and maximum front side of the dune were utilized for more precise front velocity measurement.

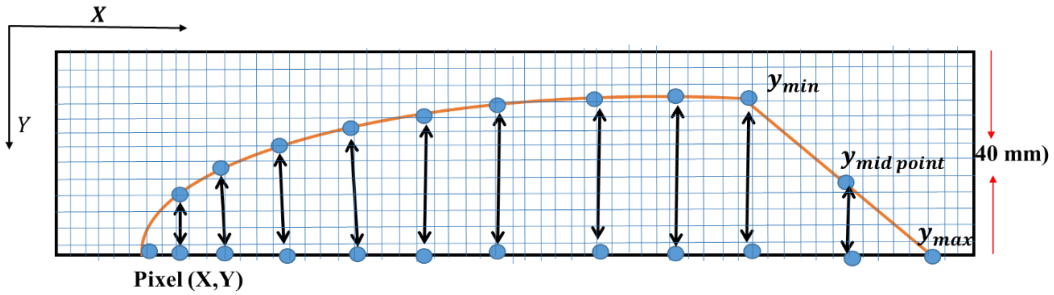

Figure 5: Block diagram for precise illustration of PIV technique

Furthermore, the tail velocity of the dune bed was computed with same manner by placing the pointer onto the desired point of the dune tail side using two different

frames with different time interval and this was done by inserting the selected frames for processing in MATALAB ‘ Image view application’. An overall summary block diagram is illustrated in Figure 5.1:

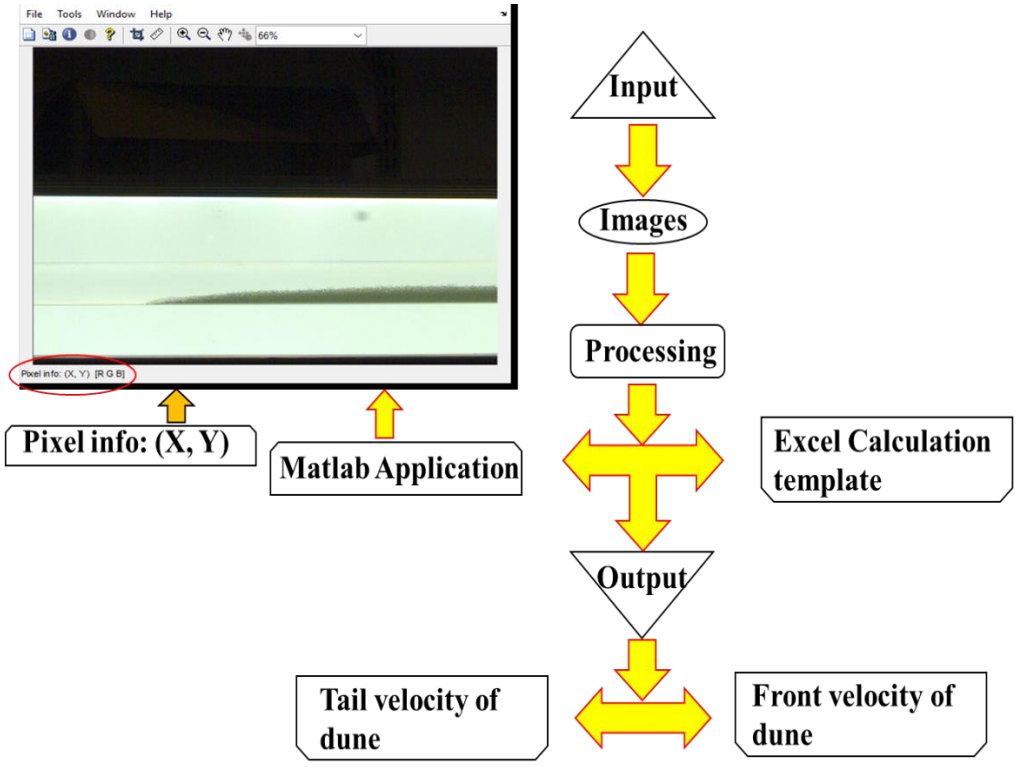

Figure 5.1: Block diagram for precise illustration of PIV technique.

2.1.3.2 Height calculation using images

The real height of the dune was computed by processing the images and frames of the dune bed at initial condition as well as in the test section. We calculated the height of the dune bed using MATLAB “image view” software. Furthermore, the length and relative area of the dune bed was formulated as well. From the image, the X and Y values were extracted by placing the pointer at each grid block of the dune bed. Initially, the diagram has been scaled to convert the pixel into cm by developing excel template with all formulation for quick output. After reading the pixels from image, the insertion of the X and Y values into the excel template has been done to find the real height, length and area of the dune more precisely. We can see Figure 5.2 in which systematic illustration for height, length and area calculation of the dune bed presented in precise manner.

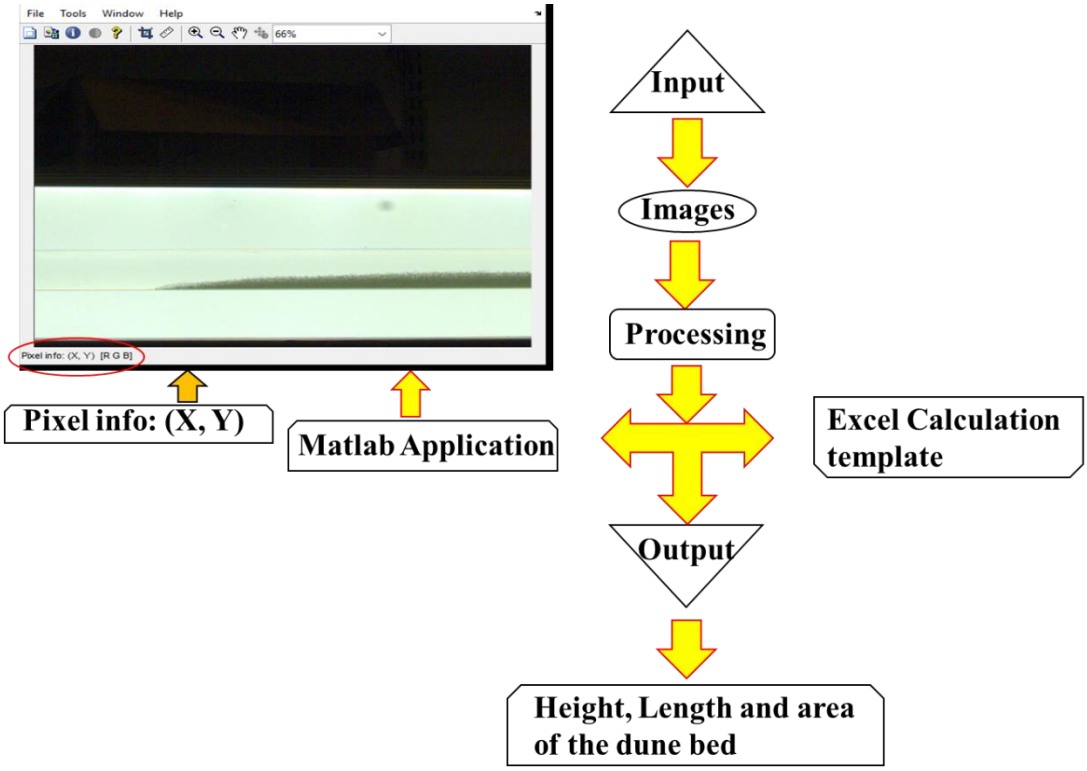

Figure 5.2: Block diagram for calculating height, length and area of the dune bed using MATLAB application.

2.1.3.3 Steps to calculate height

1. Selection of the image or frame i.e. it highly depends on which condition we are interested to find out the bed height for instance when dune bed is in stationary condition or in motion.
2. Using MATLAB application, we can insert desired image for processing. We must place the cursor to desired points of dune and read the x, y values at every point, and then we must convert the pixels into mm or cm for further calculations. We can see Figure 5.3 in which schematic illustration is presented to find the height of the dune bed.

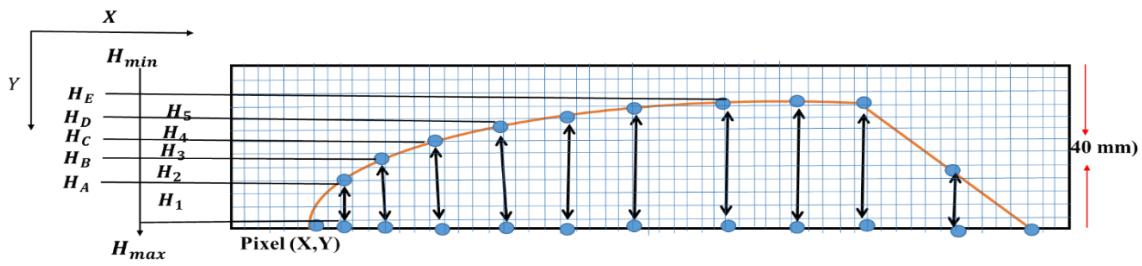

Figure 5.3: Schematic diagram of dune bed with bullet points to show the methodology of height calculation.

$$H_1 = H_{max} - H_A$$
$$H_2 = H_{max} - H_B$$
$$H_3 = H_{max} - H_C$$
$$H_4 = H_{max} - H_D$$
$$H_5 = H_{max} - H_E$$

Where

"H" is height at each section and subscript A, B, C, D E are just to show the height of dune at specific points.

After finding desired points, we can find the height at every section and we can draw the dune bed in excel sheet and we can evaluate the relative area and concentration of the dune particles where "H" is height of the dune at each point.

3. After finding height of the bed, we must compute the relative area of the dune bed.

$$\emptyset = \mathbf{Cos^{-1}}\left(\frac{r-h}{r}\right) \quad \text{(eq 11)}$$

Where

$\emptyset$ = contact angle

r = radius of the pipe

h = height of the dune bed

$$A_r = \frac{\emptyset - (\sin\emptyset * \cos\emptyset)}{\Pi} \qquad \text{(eq 12)}$$

A_r = relative area of the dune

Π = constant value (3.141)

The eq 28 and eq 29 was computed from paper written by Doron P and D. Barnea 1993.

2.1.4 Three-layer model:

Doron P and D. Barnea 1993 explained very well about three-layer model and they gave brief description about three-layer model. According to their description if we suppose two-phase solid liquid mixture flowing all together in the pipe of horizontal section and if the flow rate of the slurry is very high then all solid particles will tend to reach the suspension level and all particles will start suspending due to high flow rate. The particles with high density will settle down on the bottom of the pipe due to high weight, eventually form moving deposit, and finally flow as heterogeneous mixture. On contrary to this if, we lower the flow rate then the bed height will increase and mean velocity decreases. Based in two-layer model, when the sum of driving forces acting on bed will become smaller than the sum of opposing forces against the bed motion then the bed become stationary and will not move apart. Based on laboratory observations, it can be concluded that at low flow rates the upper layer may be moving while lower layer can remain stationary. Therefore, at low bed velocities, the particles can get stuck at the bottom and the bed is enable to drag the particles. This contributes to description of the flow by three-layer model where the bed comprises of two layers. Hence, the stationary layer height is at minimal value, which is required for particle motion. The minimal velocity that can help to rebuilt the particle motion. However, the upper part of the pipe tenanted by heterogeneous mixture.

2.1.4.1.1 Minimal bed Velocity:

To achieve the minimal bed velocity of moving layer, consider solid particle at lower most level of moving bed layer. If we see Figure 5.4, we will better understand the particles, which settle down on the trough between adjoining particles of upper section of stationary bed. However, the particle assumed to be at point or limit of rolling. In this scenario, the driving torque and opposing torque should be balance with each other. However, the driving torque appears because of drag force imposed by moving bed layer on particle and opposing torque is the result of weight of the particle and moving bed particle. The magnitude of the driving and opposing torque depends upon the velocity of moving bed layer; it can be computed from torque balance. The driving force imposed by moving layer on particles can expressed as:

$$F_D = \frac{1}{2}\rho_L U_{bc}^2 C_D A_P \quad \text{eq 13}$$

Where

F_D = Driving force (N)

ρ_L = density of carrier liquid $\left(\frac{Kg}{m^3}\right)$

U_{bc} = Critical bed velocity (m/s)

C_D = Drag coefficient of particle

A_P = Area on which drag force act on it

We can also Figure out the A_p from following equation:

$$A_P = \frac{1}{4}\pi d_p^2 - \frac{1}{8}d_p^2\left(\frac{\pi}{3} - sin\frac{\pi}{3}\right) = 0.763d_p^2 \quad \text{eq 14}$$

Where

d_p = Particle diameter (m)

π= Constant value (3.1416)

However, the torque balance is carry out for point of contact between particle and its neighbor in downstream position represented by O in Figure 5.4. The perpendicular distance to the line of action can expressed by following equation:

$$L_D = \frac{d_p}{2}\left(sin\frac{\pi}{3} + 0.0137\right) \quad \text{eq 15}$$

Where

L_D = perpendicular distance to line of action

However, the opposing torque is because of the weight of the particle and solid particle in moving bed layer that are pressing it hardly. According to this journal, the average number of solid particles computed from following correlation:

$$N = C_{mb}\frac{y_{mb} - d_p}{d_p} + 1 \qquad \text{eq 16}$$

Where

N = Average number of solid particle in moving layer

C_{mb} = Moving bed concentration (according to Doron and barnea journal C_{mb} =0.52 for close packing)

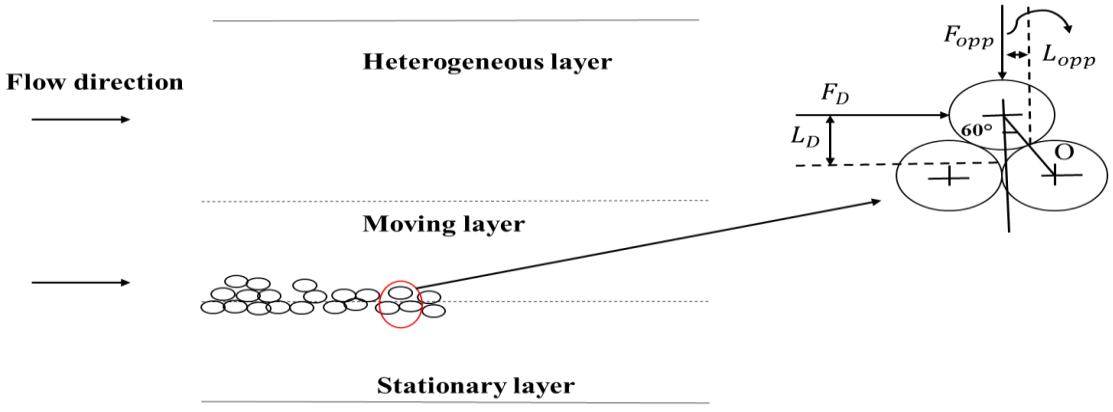

Figure 5.4: Forces acting on the particle at the upper stratum of stationary bed (Doron P and D. Barnea 1993 edited by myself)

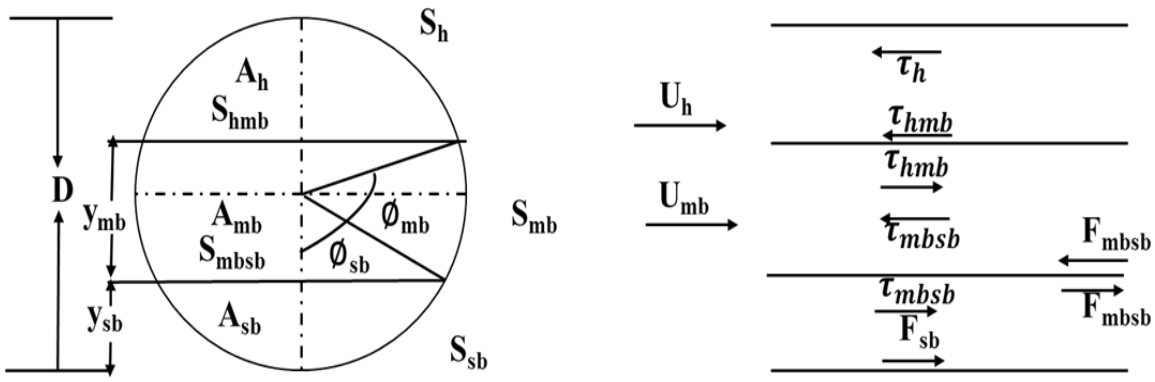

Figure 5.5: Schematic illustration of three-layer model; geometry, velocities and shear stresses (Doron P and D. Barnea 1993 edited by myself)

The submerged weight of the particle can be presented by following correlation:

$$W_p = \frac{1}{6}\pi(\rho_s - \rho_L)g d_p^3 \qquad \text{eq 17}$$

Where

g= gravitational acceleration (m/s^2)

Moreover, the opposing force can be expressed by:

$$F_{opp} = W_p\left[C_{mb}\frac{y_{mb}}{d_p} + (1 - C_{mb})\right] \qquad \text{eq 18}$$

Where

Y_{mb} = height of moving bed

However, the perpendicular distance to the point of action of opposing force can be presented for better conceptions:

$$L_{opp} = \frac{d_p}{2} sin\frac{\pi}{6} \qquad \text{eq 19}$$

$$\tau_D = F_D L_D \qquad \text{eq 20}$$

$$\tau_{opp} = F_{opp} L_{opp} \qquad \text{eq 21}$$

Where

τ_D = Driving torque

τ_{opp}= opposing torque

After equating equation i.e. opposing torque and driving torque, we will end up with following correlation:

$$U_{bc} = \sqrt{\frac{0.779(\rho_S - \rho_L) g d_p \left[C_{mb}\frac{y_{mb}}{d_p} + (1 - C_{mb})\right]}{\rho_L C_D}} \qquad \text{eq 22}$$

Where

U_{bc} = Velocity of moving bed (m/s) for which particles are at the bottom of the section and almost is at limit of rolling

Anyhow, according to doren and barnea journal when the slurry flow rate is reduced then the mean velocity U_b decreases as well and if it becomes smaller than U_{bc} then stationary layer will start appearing. Further decrement in slurry flow rate can form stationary layer and decrease the moving bed height. However, the U_{bc} decrease comparatively when slurry flow rate is reduced **(**Doron P and D. Barnea 1993).

Doron and barnea explains about three-layer model by assuming that if solid and liquid is flowing all together in the horizontal pipe flow then there will form three layers; stationary layer, moving layer and heterogeneous layer. It can be seen in Figure 5.5.

2.1.4.1.2 Continuity:

Two continuity equations are presented below:

For soild particles, $$U_h C_h A_h + U_{mb} C_{mb} A_{mb} = U_s C_s A \qquad \text{eq 23}$$

And for liquid phase, $$U_h(1 - C_h)A_h + U_{mb}(1 - C_{mb})A_{mb} = U_s(1 - C_s)A \qquad \text{eq 24}$$

Where

U_h = heterogeneous upper layer axial velocity

C_h = C denotes volumetric concentration of solid particles and subscript “h” denotes heterogeneous upper layer

A_h = pipe cross sectional area and subscript “h” denotes heterogeneous upper layer

In addition, subscript “mb” denotes moving bed in above equations.

U_s = Slurry superficial mean velocity

C_s = Slurry input concentration

A_h = Cross sectional area occupied by dispersed layer

A_{mb} = Cross sectional area occupied by moving layer

2.1.4.1.3 Momentum:

Force balances can be presented for three layers. For dispersed upper layer, the heterogeneous mixture can be assumed as pseudo liquid.

$$A_h \frac{dp}{dx} = -\tau_h S_h - \tau_{mb} S_{mb} \qquad \text{eq 25}$$

Where

$\frac{dp}{dx}$= Pressure drop

τ_h = shear stress at the pipe circumference

τ_{mb} = interfacial shear stress

S_h = interface of disperse layer

S_{mb} = interface of moving layer

However, the shear stress at the pipe circumference can be found from following equation:

$$\tau_h = \frac{1}{2}\rho_h |U_h| U_h f_h \qquad \text{eq 26}$$

The shear stress at the upper layer and moving bed can be presented by following equation:

$$\tau_{hmb} = \frac{1}{2}\rho_h |U_h - U_{mb}| (U_h - U_{mb}) f_{hmb} \qquad \text{eq 27}$$

ρ_h = Effective density of upper layer

f_{hmb} = friction coefficient at pipe wall and moving layer

U_{mb} = axial velocity of moving layer

The Effective density of upper layer can be computed as:

$$\rho_h = \rho_s C_h + \rho_L (1 - C_h) \qquad \text{eq 28}$$

Where

ρ_s = Density of solid particles (kg/m^3)

ρ_L = Liquid density (kg/m^3)

C_h = "C" denotes volumetric concentration of solid particles and subscript "h" denotes heterogeneous upper layer

The coefficient of friction at the wall of the pipe can be expressed as:

$$f_h = \propto_h Re_h^{-\beta_h} \qquad \text{eq 29}$$

Where

$\propto_h$ = 0.046, β_h = 0.02 for turbulent flow

$\propto_h$ = 16, β_h = 1 for laminar flow

(Doron P and D. Barnea 1993

3 Experimental work

The experimental work was done in Multiphase Laboratory in University of Stavanger with all reserved rights. However, in this part we would like to give the brief introduction about medium scale flow loop, which was already built. In addition, the PIV (Particle image velocimetry) were already organized with LED for light and high-speed cameras to capture images of the dune bed. Although, the experimental setup is very crucial to explain with precise measurements about the length and diameters of the pipes and the quality of the pipes including roughness factor. We will explain briefly about PIV, which we used to calculate the velocity of the particles, and off course, two camera high-speed cameras were used to capture the particles movements using light sheet.

A realistic Multiphase Laboratory can be viewed in Figure 6:

Figure 6: Real view of Multiphase Lab in University of Stavanger.

1= 5-degree section of the pipeline

2= horizontal section of the pipeline

3= DP sensor (Differential pressure sensor)

4 = Pump

5=Computer used to operate the logging system

3.1 Experimental facility

Figure 7 is the schematic diagram of medium scale flow loop in the Multiphase Laboratory University of Stavanger. Although, we have labeled the number as reference and explained each section below Figure 7. Figure 8 is real 3-D illustration of horizontal section of the medium scale flow loop. As our main area of interest was to investigate the rheology of the fluid particle in horizontal section of the pipe. Furthermore, the length of horizontal section is 1.52m and inner diameter of the pipe is 40mm. Two pressure taps (PH-High pressure side and PL-Low pressure side) are connected to differential pressure sensor to measure the pressure gradient through LabVIEW software using computer. The medium scale flow loop in Multiphase Laboratory was already settled up for making different experiments. However, the transparent glass pipes were used in this flow loop. The inner diameter of the pipe is 40 mm and the wall thickness of the pipe is about 2.3 mm. The entire length of the flow loop is about 14 m flat. This flow loop is closed circuit flow loop because we want to keep the pressure and amount of the particles inside the pipe constant so that is why it is also called closed circuit flow loop. However, the flow loop comprises of four different test sections.

1. Horizontal test section
2. Inclined 5-degree test section
3. Inclined 35-degree test section
4. Bend section

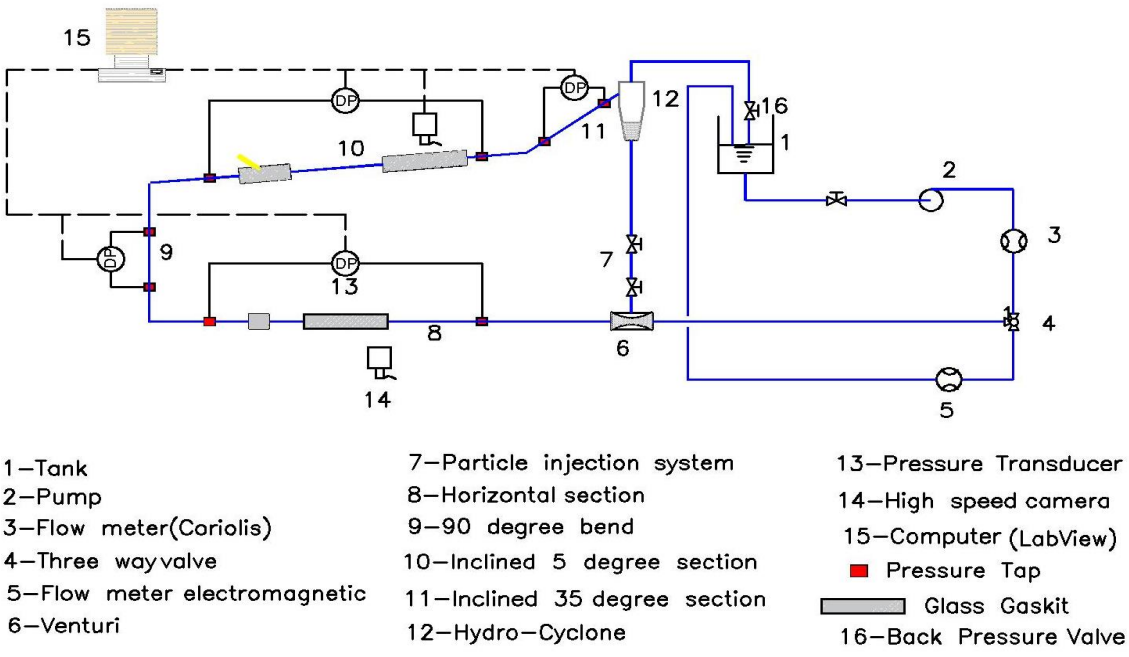

Figure 7: Schematic diagram of medium scale flow loop of Multiphase Lab in University of Stavanger.

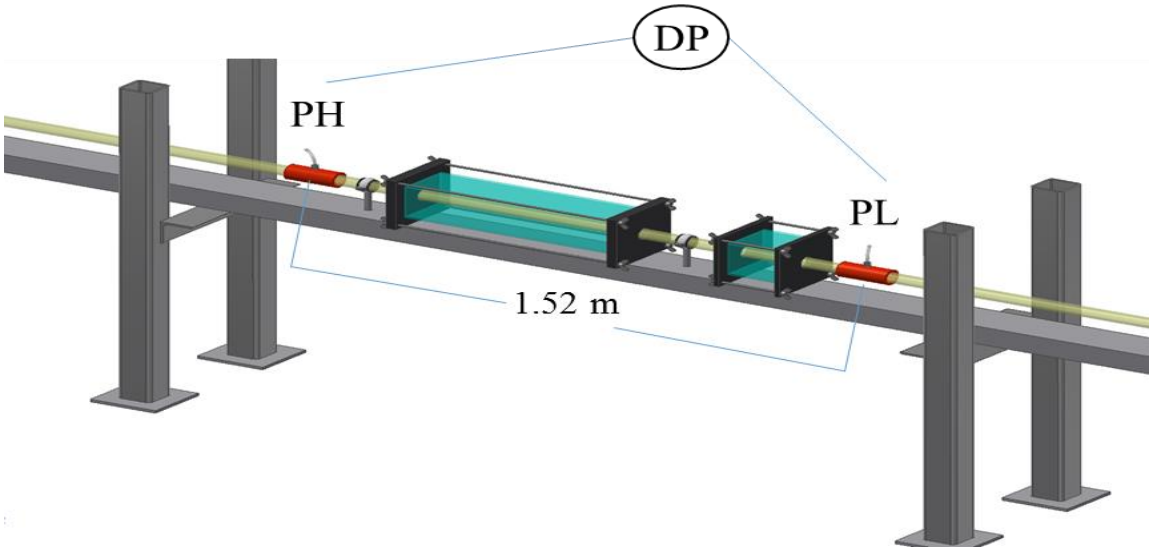

Figure 8: 3-D illustration of horizontal section of medium scale flow loop of Multiphase Lab in University of Stavanger.

The thesis was based on cutting transportation in horizontal test section. However, in flow loop of every test section two pressure taps are connected, one is high-pressure side, other one is low-pressure side, and each pressure tap is connected to pressure transducer to measure the differential pressure. This procedure is controlled by the program called LabVIEW in the computer through which we found the pressure drop as function of time and mass flow rate in kg/hr through Coriolis flow meter. In this lab, screw pump was used to pressurize the fluid in flow loop continuously. Frequency converter setup is used to control the superficial velocity of the liquid and mass flow rate through device called Coriolis flow meter.

3.2 Experimental Methodology

We would like to give brief introduction about how procedure was done before initializing the experiment. The first thing that we did, was to check that everything was functional, it means that there must be no leakage around the pipes and making sure that there was no bubble in pressure taps which could distort the pressure gradient values easily. To avoid this problem, flushing system was utilized, which allowed us to remove the bubbles from the pressure taps. A small pipe, which is connected to tap water and each pressure tap in all test sections and different valves to remove the bubble separately in each test section. (Anyhow, if we want to perform single phase (only water) then we do not care about particles injection from hydro-cyclone because water is coming from tank through screw pump in the test section. However, if we would like to perform the two phase (Liquid-Particle flow) then we must be careful doing particle injection through hydro-cyclone).

Particles were injected through two controller valves and there was Venturi inside the pipe, which allowed the liquid to mix with the particles and flow together. The liquid-particle mixture flowed towards horizontal test section which permitted us to see the dune of the particle moving towards high-pressure side as the dune reached to high-pressure side pressure gradient was recorded through LabVIEW program along with density and real mass flow rate and when the dune bed reached to low pressure side. The pressure gradient was recorded as well through LabVIEW program in computer. Then dune bed moved towards the bend section (90-degree) and inclined section (5-degree). In this section, there will be annular flow because we have rotating drill string inside the pipe. Finally, the flow moved towards the last section, which is 35- degree. Eventually flow approached to hydro-cyclone. Particles were settled down to hydro-cyclone due to gravitational force and liquid went back to tank (reservoir). To be sure, that particles do not go towards tank, there is secondary separator, which is placed inside the tank to collect the incoming particles as they could block the pipe and effect the screw pump badly. Therefore, we must be sure that particle will remain in hydro-cyclone injection system. To see the particle movement, we have installed the PIV system with two cameras (A Basler A800-510um color (500 fps (frame per second) with full resolution 800×600 camera) connected to computer software. Using MATLAB software, images processing was done to see particle movement. In addition, particle travelling velocity and height of the dune bed was computed as well. Some time while injecting the particles again in test section, problems were experienced because two valves can be very hard to operate. What we can did, we lowered the frequency (flow rate) through frequency converter and injected particle that could be easy to operate the valves and inject the particles into the test section. After collecting desired parameters (pressure gradient, particle velocities and height), processing was done using MATLAB application and excel format for quick output. A brief summary of technique is presented in Figure 9.0 for clear understanding.

3.2.1 Summary of technique

A brief description of experimental technique followed while performing experiments is presented in Figure 9.0.

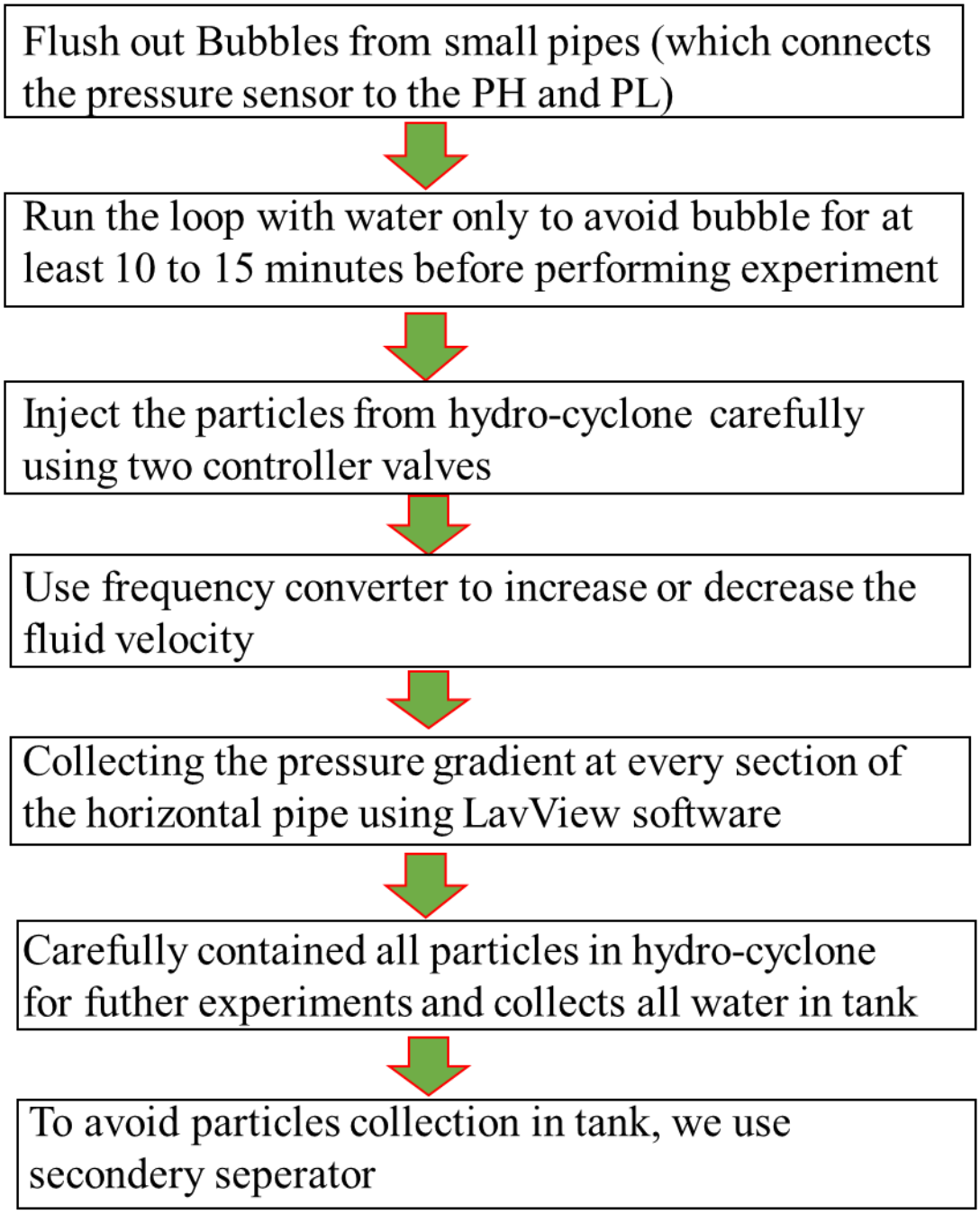

Figure 9.0: Summery of the technique used during experimentation

3.2.2 Distribution of the particles with average value of particle diameter in mm

The particle measurement is done microscopically for more accurate and precise results. Few amount of particles were collected in small container for measurement. A highly accurate microscope was used in this experiment to capture the particles which enabled us to see the particles more clearly. In addition, images of the particles were taken for further processing but before that the image was properly scaled for better processing. The processing was done in MATLAB software through "image view" application. Desired image was inserted into the MATLAB software and measurement of each particle diameter was done precisely. Three measurements were taken in each particle for better results. However, Table 1.0 is enriched with all parameters with closely accurate output and Figure 9.1 is real image of particle, which was taken under microscopic assistance. A red line on Figure 9.1 indicates the maximum scale, which was measured through microscopic assistance.

Table 1.0

Number of particle measurements	Average particle diameter (mm)	Standard deviation
804	1.1479	± 0.10431

Table 1.0: Measurement of the particle diameter used in experiment of medium scale flow loop in Multiphase Lab University of Stavanger.

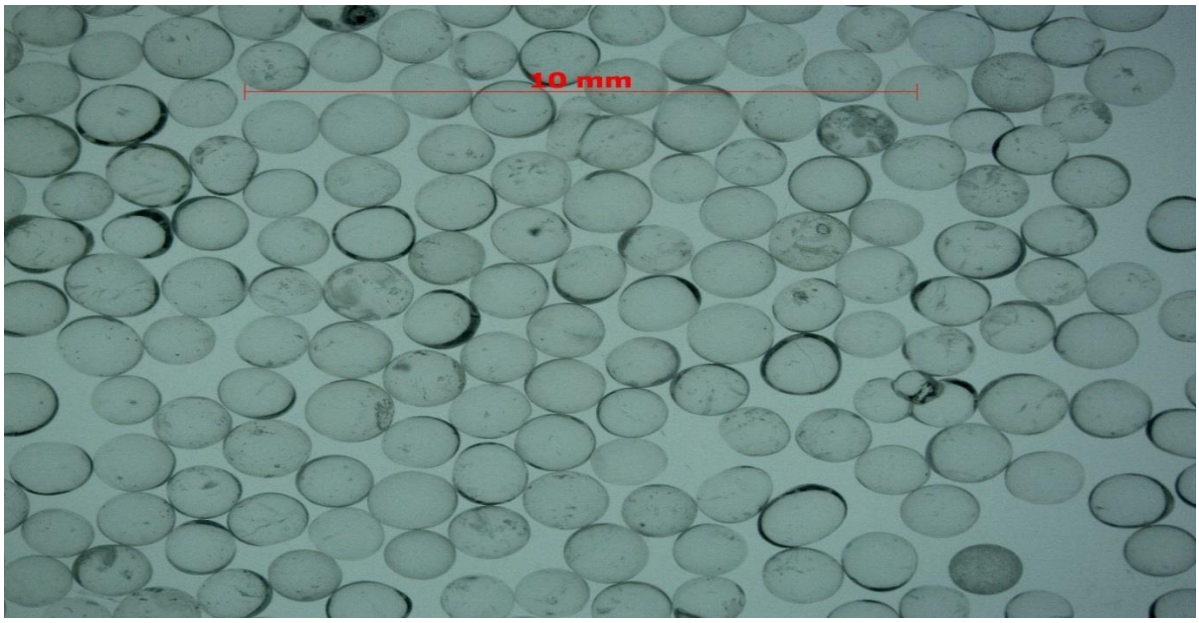

Figure 9.1: Real illustration of the particles captured through highly accurate microscope.

3.3 Test Matrix:

In this section, Table 1.1, the medium scale loop measurement with pipe inner and outer diameter, type of fluid, particle size, and camera specification is precisely illustrated for better justification of experimental procedure. The Table 2 gives comprehensive knowledge about number of experiments performed with different superficial liquid velocities and pressure gradients in each section separately.

Table 1.1

Experimental specifications of medium scale flow loop		
1	Pipe inner diameter (m)	0.040
2	Length of flow loop (m)	14
3	Fluid type	Water
4	Particle type	Spherical shape glass particles
5	Average Particle diameter (mm)	1.1479
6	Camera	A Basler A800-510um color (500 fps (frame per second) with full resolution 800×600 camera) High speed camera
7	Pressure transducer (range) mbar (mili bar)	± 62

Table 1.1: Specification of the experiment of medium scale flow loop in Multiphase Lab University of Stavanger.

Table 1.1 comprises of experimental specifications of medium scale flow loop with different parameters. Table 2 illustrates number of experiments performed during entire master thesis. Although, four experiments were performed on single phase and liquid particle flow. However, results from experiment 2 were invalid. Experiment 3 and 4 illustrated similar and trust worthy results. Therefore, we used these experiments for processing and evaluation.

Table 2

Experiment	U_{SL} (m/s)	Average DP/DL(Single phase) (Pa/m)	Average DP/DL(Liquid –particle flow) (Pa/m) reaching to single phase	Dune front velocity (m/s)	Dune tail velocity (m/s)
1	0.32	28.59	37.45	0.01107	0.004256
	0.45	68.06	68.27	0.02984	0.01705
	0.51	-	-	-	
2	0.32	Results from experiment 2 was not valid			
	0.45	Results from experiment 2 was not valid			
	0.51	Results from experiment 2 was not valid			
3	0.32	28.59	28.99	0.0053	0.00518
	0.45	68.06	68.56	0.02898	0.03092
	0.51	-	91.82	0.05056	0.05253
4	0.32	28.59	28.99	0.0053	0.00518
	0.45	68.06	68.56	0.02898	0.03092
	0.51	-	91.82	0.05056	0.05253

Table 2: Results of four experiments with different parameters

4 Results and discussion

In this chapter, results and discussions of various experiments are unfolded on transportation of particles using water in the horizontal section of the pipe flow. However, four experiments were performed to achieve the best possible results for post processing of the data. Therefore, three scenarios were selected from different experiments. Anyhow, the thesis was based on cutting transport in horizontal section of medium scale flow loop, so our results belongs to horizontal section of the pipe.

However, the total pressure drop comprises of pressure loss due to friction, Hydrostatic pressure loss and pressure drop due to acceleration. As we can see in eq 30:

$$\left(\frac{DP}{DL}\right)_{Total} = \left(\frac{DP}{DL}\right)_{friction} + \left(\frac{DP}{DL}\right)_{acceleration} + \left(\frac{DP}{DL}\right)_{Hydrostatic} \quad \text{(eq 30)}$$

As in this thesis, we are focusing on horizontal section of the pipe. Therefore, in the case of horizontal section, we do not have hydrostatic pressure loss so we neglect the hydrostatic term as in eq 31:

$$\left(\frac{DP}{DL}\right)_{Total} = \left(\frac{DP}{DL}\right)_{friction} + \left(\frac{DP}{DL}\right)_{acceleration} + \cancel{\left(\frac{DP}{DL}\right)_{Hydrostatic}} \quad \text{(eq 31)}$$

So finally, we end up with this eq 32:

$$\left(\frac{DP}{DL}\right)_{Total} = \left(\frac{DP}{DL}\right)_{friction} + \left(\frac{DP}{DL}\right)_{acceleration} \quad \text{(eq 32)}$$

In addition, through this equation, the pressure gradient can be computed in pipe flow in the horizontal section of the pipe. Although, the pressure drop due to friction and acceleration is apparent in results and discussion in scenario 1, 2 and 3 as following:

a) Scenario 1 - U_{SL}=0.32 m/s
b) Scenario 2 - U_{SL}=0.45 m/s
c) Scenario 3 - U_{SL}=0.51 m/s

Different superficial liquid velocities were utilized to observe different behavior of pressure gradient and to analyze the rheology of the fluid flowing together with particles.

4.1 Experimental analysis of cutting transportation in horizontal section using Newtonian fluid (water) with different superficial liquid velocities:

4.1.1 Scenario 1 using superficial liquid velocity (U_{SL}=0.32 m/s)

In Figure 10a, 10b and 10c, the X-axis contains Pressure gradient in (Pa/m) and y-axis comprises of time in second. However, the title of these Figures is pressure gradient as function of time. Figure 10a consists of liquid particle flow, Figure 10b indicates single-phase flow and Figure 10-c is the combined illustration of single phase and liquid particle flow. Figure 10d is the illustration of dune height as function of length in cm where A_rel is relative area of the dune bed. In Figure 10d, the x-axis contains height in cm and y-axis consists X values which is the length of the dune in cm. However, in Figure 10d, three cases are mentioned (Initial stationary, initial condition moving and test section). Initial stationary condition means that dune is stationary at initial conditions, initial condition moving means when dune starts moving at initial condition and test section is main area of interest. Figure 15-e is real dune illustration at initial condition and Figure 15f is dune illustration at test section. Front and tail velocities are also mentioned. To explain more precisely, the sectioning with label A, B, C, D and E is done in Figure 10a.

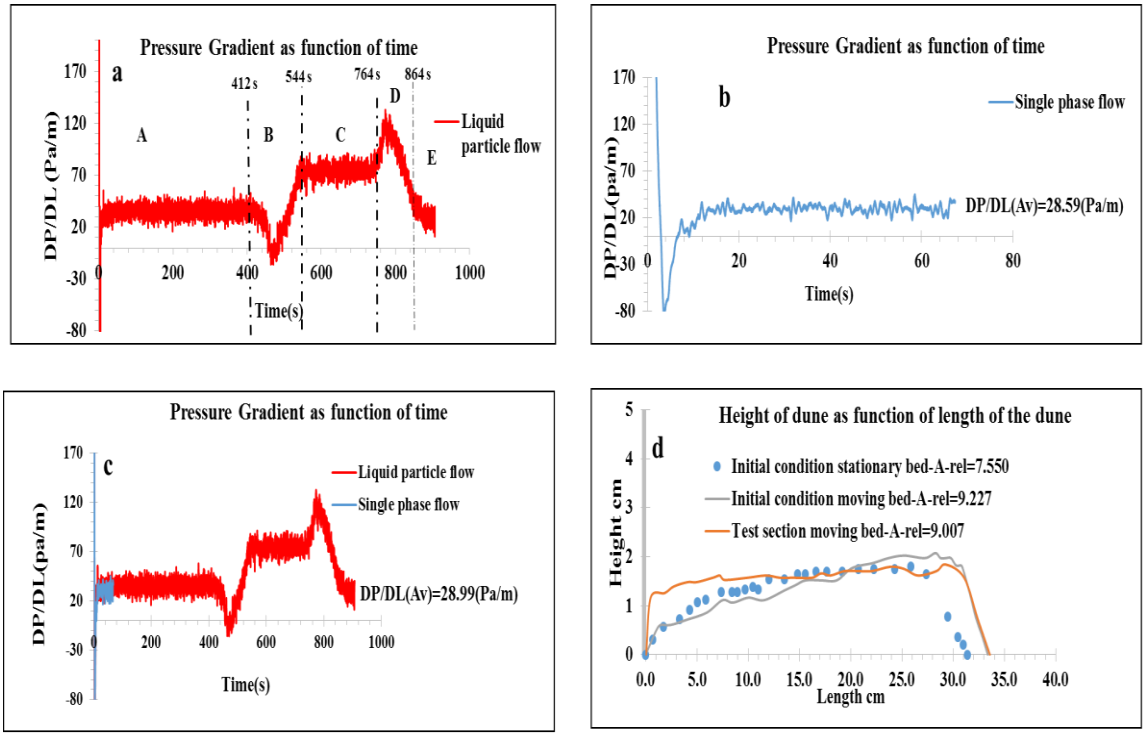

Figure 10: Results of pressure gradients. a)- Liquid-Particle flow. b) - Single-Phase flow. c) - Combine illustration of a,b where d)- Dune height as function of length

Where

DP/DL (Av) = Average Pressure gradient (Pa/m) reaching to single phase (Figure 10-c)

A_rel = Relative area of the dune bed

4.1.1.1 Analysis of pressure gradient as a function time

In section A, Figure 10-a, the dune is at initial condition it means that we were not recording the pressure gradient at this section so the flow was in single phase. A schematic diagram illustrations are presented in Figure 11g and 11h for better understanding:

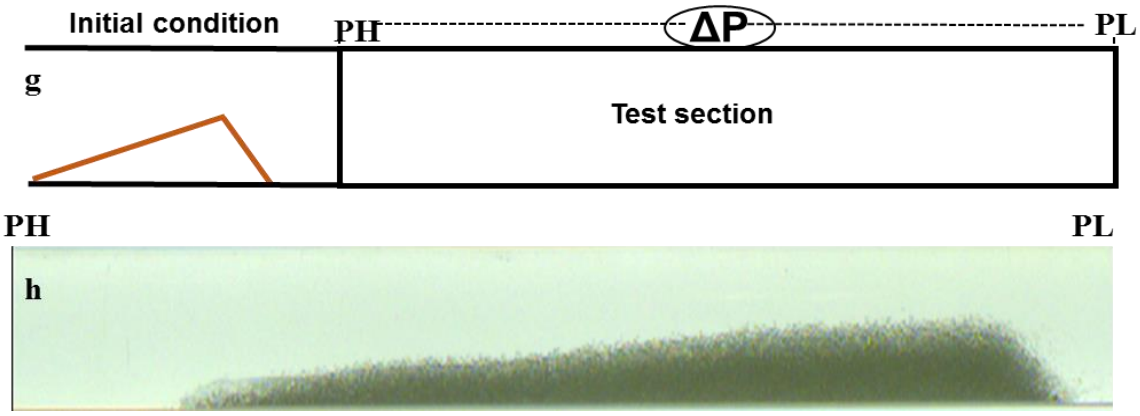

Figure 11: Pipe illustration with initial condition and test section. g)-schematic diagram showing dune is @ initial condition and h)-real dune Figure moving in at initial conditions (section A).

It is apparent that the dune was at initial condition just behind the test section so flow was in single phase. However, PH is high-pressure side and PL low-pressure side. Furthermore, Figure 11g shows the pipe flow with initial condition and test section (where we want to measure pressure gradient) whereas Figure 11-g is schematic diagram of dune when it is at initial condition and Figure 11-h is real dune illustration in initial conditions.

In section B, Figure 10a, the dune reached to high-pressure side (PH), the decline in pressure gradient is apparent in this region, and this is due to Bernoulli effect. Although, there was the effect of friction and turbulences in this section but Bernoulli effect is more pronounced in this section. Anyhow, when the dune bed reached to the PH (high-pressure side), the flow area above dune bed of the pipe has been reduced due to which PH decreased (PL remains constant) and velocity increased and eventually pressure gradient decreased, which is related to equation 34:

$$P + \frac{1}{2}\rho\, v^2 = \text{constant} \quad \text{(eq 33)}$$

P = Pressure (Pa)

ρ = density (kg/m^3)

v = velocity (m/s)

$$\Delta p = P_H - P_L \text{ (eq 34)}$$

Δp = Pressure difference (Pa)

P_H = High-pressure side of the test section (changing)

P_L = Low-pressure side of the test section (constant)

After decline, the pressure gradient is increased because of the frictional pressure drop due to particle-particle interaction, particle-wall interaction and liquid against particle. In addition, there is effect of turbulence and vortexes (it is region where flow rotates around its axis) that can cause pressure gradient to increase. We can see Figure 12i and 12j, the schematic diagram of the dune and real dune illustration below reaching PH (high-pressure side).

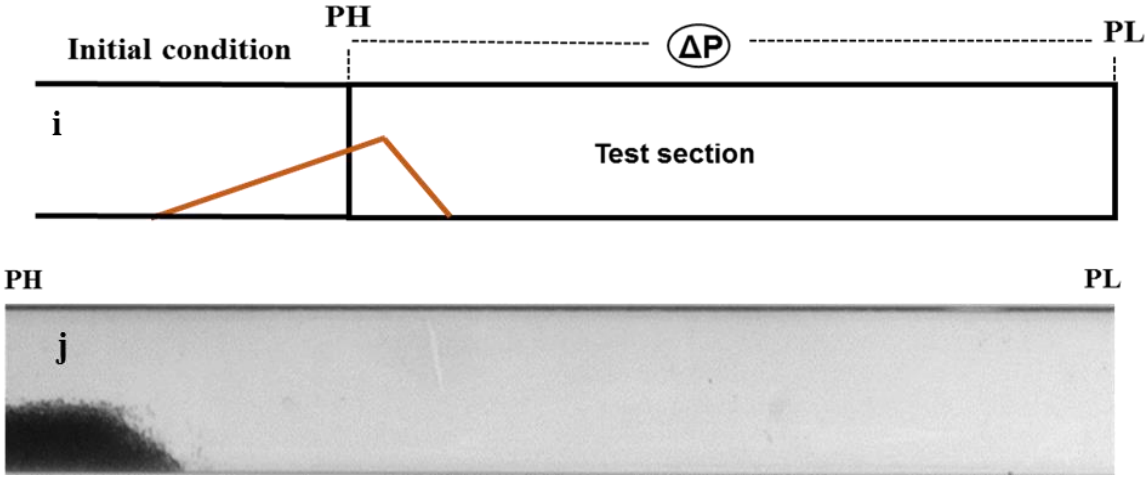

Figure 12: Pipe illustration with initial condition and test section. i)-schematic diagram showing dune is at PH and j)-real dune Figure at PH (high-pressure side) (Section B).

In section C, Figure 10-a, the dune is now in the test section and pressure gradient is somehow stable in this region, this is because in this region, the dune was moving into the test section and there is frictional pressure drop due to particle-particle interaction, particle-wall interaction and liquid against particle. In addition, the effect of turbulence and vortexes (it is region where flow rotates around its axis) was also pronounced in this section that could cause pressure gradient to change. The dune particles were shearing the wall of the pipe casing high friction. The friction between particle wall, liquid particle and liquid wall can cause high friction, which eventually results change in pressure gradient. This is related to Darcy Weisbach equation:

According to Darcy Weisbach model:

$$\frac{\Delta p}{L} = f_{\mathrm{D}} \cdot \frac{\rho}{2} \cdot \frac{\langle v \rangle^2}{D}, \quad \text{(eq 35)}$$

ΔP = Pressure (Pa/m)

ρ = density (kg/m^3)

v = velocity (m/s)

L= Length (m)

f_D = Darcy friction factor

D = Inner diameter of the pipe (m)

To summarize, it is quite realistic to say that in section C, we can have three effects that can cause change in pressure gradient:

1) Movement of the dune bed inside the test section
2) Frictional pressure drop due to particle-particle interaction, particle-wall interaction and liquid against particle.
3) Effect of turbulences of flow at dune front.

Figure 13-k and 13-l indicates that dune is in the test section:

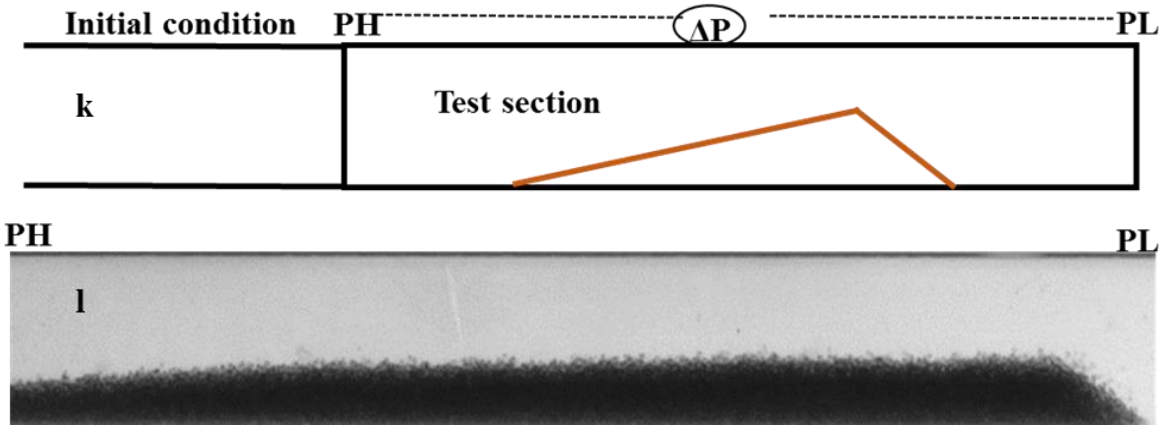

Figure 13: Pipe illustration with initial condition and test section. k)-schematic diagram showing dune is in test section and l)-real dune Figure in the test section (Section C).

In section D, Figure 10a, pressure gradient increased due to Bernoulli effect because dune was now at low-pressure side (PL) so flow area decreased due to which PL decreased as well (while keeping PH constant) and velocity increased and eventually pressure gradient increased based on equation 34. Finally, after some time, the pressure gradient started decreasing because now particles were washed out from the test section. This can be justified better by schematic diagram Figure 14m and 14 n.

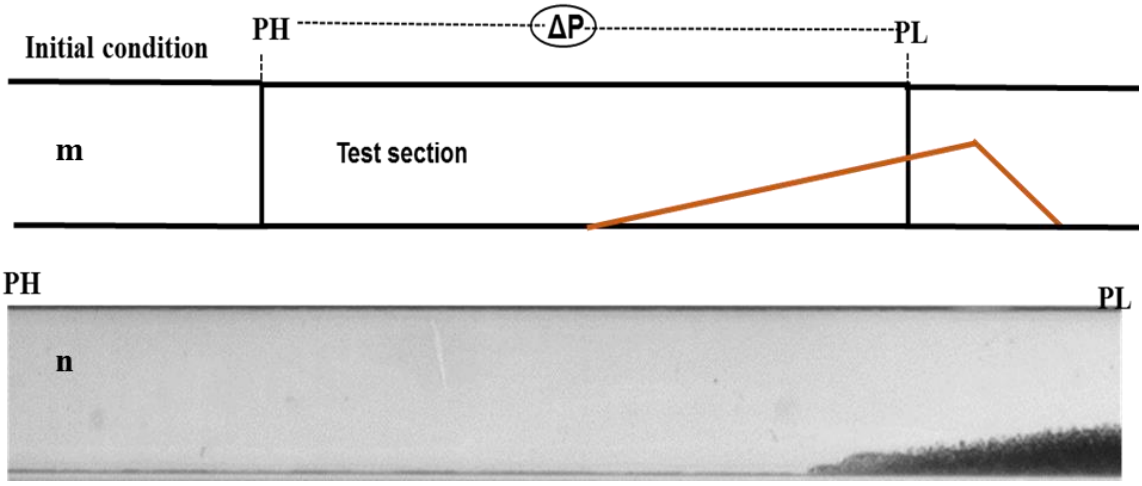

Figure 14: Pipe illustration with initial condition and test section. m)-schematic diagram showing dune is is at Low-pressure side and n)-real dune Figure is at PL (low-pressure side) (Section D).

Finally, in section E Figure 10a, the particles were now washed out. There was single-phase flow in pipe.

4.1.1.2 Analysis of bed height, length and particle velocities:

Figure 10-d is the combined illustration of three cases (initial stationary condition, initial condition moving and test section). However, in Figure 10d, the height of the bed at initial stationary and moving condition was higher than the dune height in the test section. The length of the dune in test section was larger than length of the dune at initial stationary condition. Although length of the dune in initial moving condition and in test section was quite similar with minor differences. This is because the velocity of the dune front was bit larger than tail velocity of the dune so the whole dune was expanding due to which the increased in the dune length in test section was apparent as it can be seen in Figure 15-e and 15-f. However, Front velocity (V_front) of dune was 5.30 mm/s and tail velocity (V_tail) of dune was recorded about 5.18 mm/s. In addition, the dune bed was quite smooth with less scoring and suspended particles. From Figure 10d, it is confirmed that the relative area (A_rel) of the dune bed in stationary condition was smaller compare to initial moving and test section condition. This is because when the dune bed is at initial stationary condition, it is more packed (particles are tightly packed together) but in case of initial moving and test section condition, the dune is now moving, which allow the particles to spread around and there will be water inside the pore spaces of the particles.

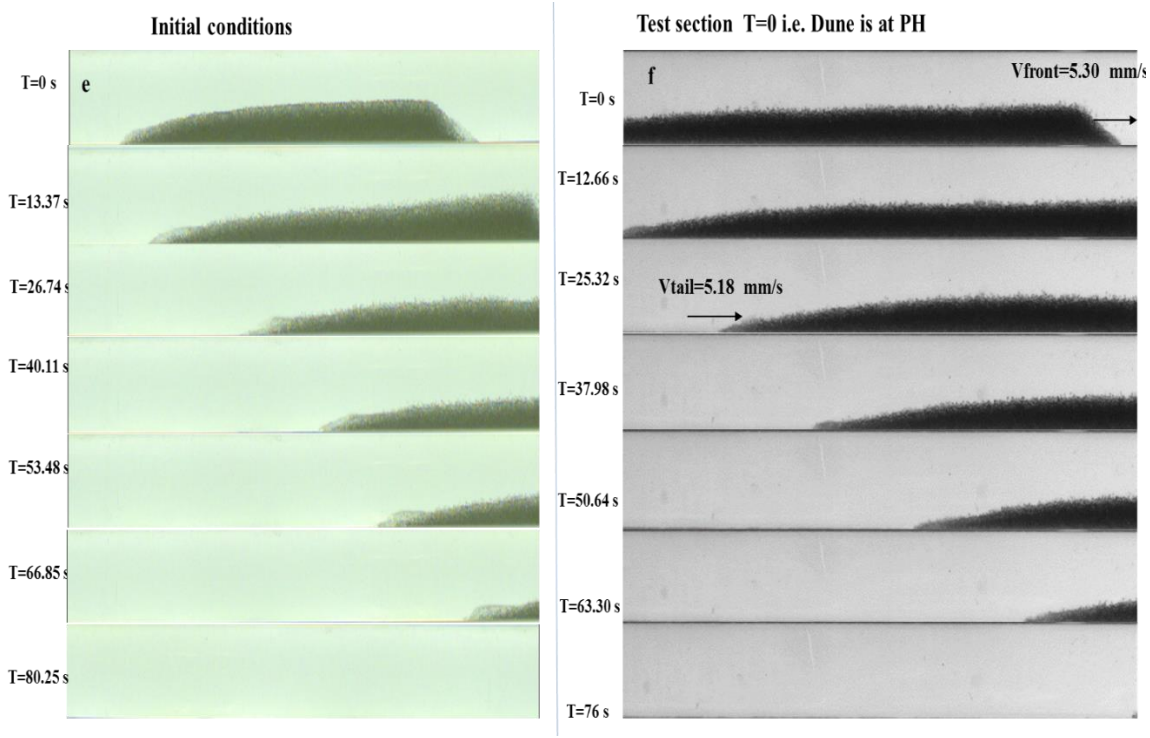

Figure 15: Real illustration of dunes. e)-Initial conditions. f)-Test section

4.1.1.3 Key points

a) At low flow rate or U_{SL}=0.32 m/s, the particles flushing out slowly from the horizontal section of the pipe. The dune bed is quite smooth.

b) The velocity of the dune front is higher than velocity of the dune tail.

c) The height of the dune bed has decreased as dune reached to the test section; this is because of the high dune front velocity due to which the dune is expanding causing increase in the length of the dune.

4.1.2 Scenario 2 using superficial liquid velocity (U_{SL}=0.45 m/s)

In Figure 16o, 16p and 16q the X-axis contains Pressure gradient in (Pa/m) and y-axis comprises of time in second. The title of these Figures is pressure gradient as function of time. Figure 16-O comprises of liquid particle flow, Figure 16p illustrates single-phase flow and Figure 16q is the combined illustration of single phase and liquid particle flow. Figure 16r is the illustration of dune height as function of length in cm. The x-axis contains height in cm and y-axis consists length of the dune in cm. However, three cases were combined in graph (Initial stationary condition, initial condition moving and test section). Initial stationary means that dune is stationary at initial conditions; initial condition moving means when dune starts moving at initial condition and test section is main area of interest. In addition, Figure 21s is real dune illustration at initial condition and Figure 21t is dune illustration at test section. Front and tail velocities are also mentioned in Figure 21t.

However, in this case it is quite apparent to see in Figure 16-O that cutting are being washed out faster than previous case (ULs=0.32 m/s). Moreover, the sectioning has been done for précised illustration of the Figure 16-O.

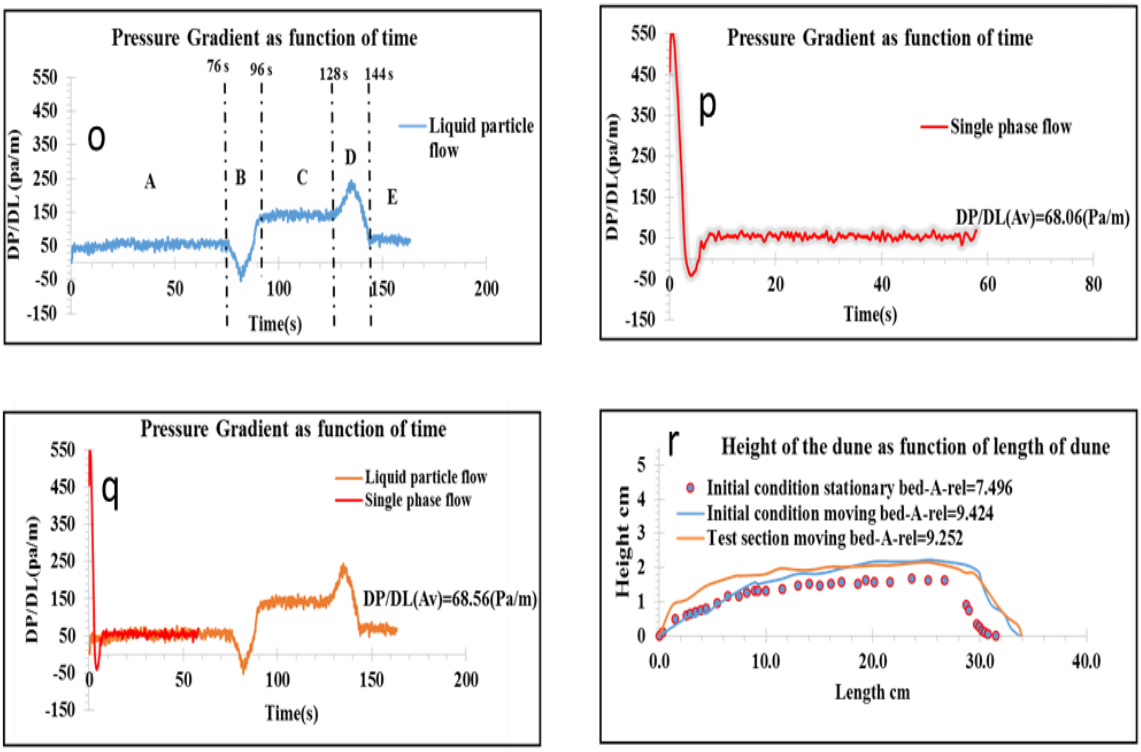

Figure 16: Results of pressure gradients. o) - Liquid-Particle flow. p) - Single-Phase flow. q) - Combine illustration of o,p where r)- Dune height as function of length.

Where

A_rel = Relative area of the dune bed

DP/DL (Av) = Average Pressure gradient (Pa/m) reaching to single phase (Figure 16-q)

4.1.2.1 Analysis of pressure gradient as a function time

In section A, Figure 16-O, Dune is at initial condition just behind the test section so this section there will be single-phase flow in pipe as it has been unfolded in Figure 17u and 17v:

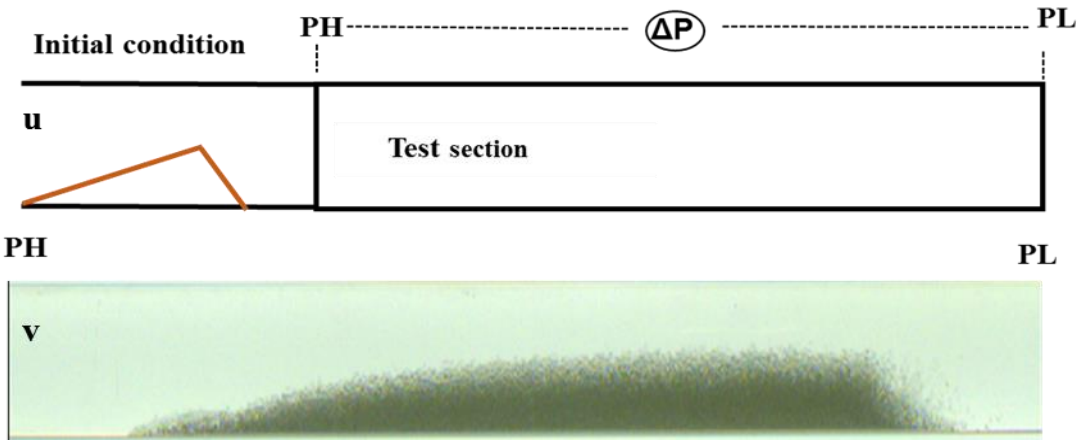

Figure 17: Pipe illustration with initial condition and test section. u)-schematic diagram showing dune is @ initial condition and v)-real dune Figure moving in at initial conditions (section A).

In section B, Figure 16-O, dune bed was at high-pressure side and pressure gradient decreased this is again because of frictional and turbulence effect but Bernoulli effect was more pronounced in this section. Because when the dune reached to high-pressure side (PH), the cross-sectional area of the pipe reduced due to which velocity increased and PH reduced (while keeping PL constant), eventually pressure gradient decreased sharply based on equation 34. All sudden pressure gradient started increasing this is because of the frictional Effect and vortexes (flow rotates around its axis) and turbulences of flow at dune front as we can see Figure 18w and Figure 18x.

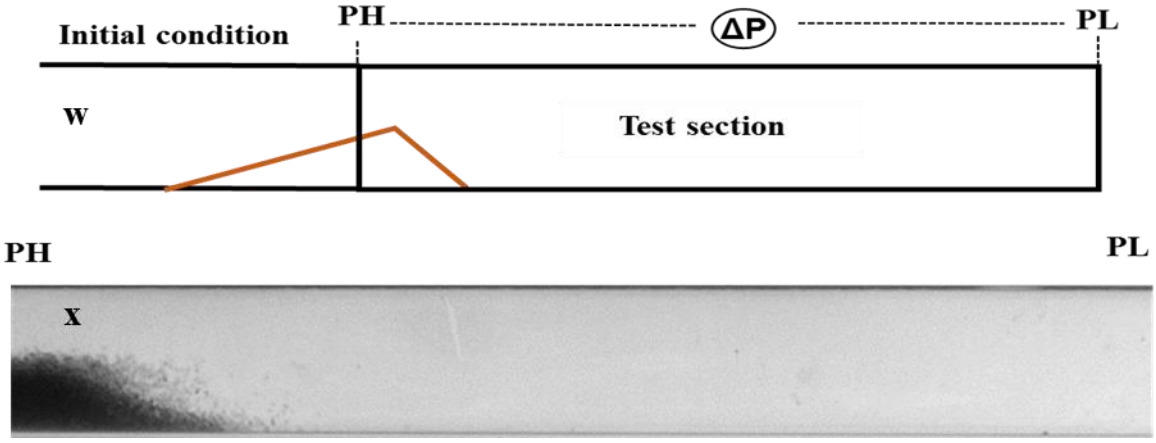

Figure 18: Pipe illustration with initial condition and test section. w)-schematic diagram showing dune is at PH and x)-real dune Figure at PH (high-pressure side) (Section B).

In section C, Figure 16-O, the dune is in the test section and pressure gradient is stable in this section, this is because of following reasons:

1) Movement of the dune bed inside the test section
2) Frictional pressure drop due to particle-particle interaction, particle-wall interaction and liquid against particle.
3) Effect of turbulences of flow at dune front.

We can understand better by Figure 19y and 19z.

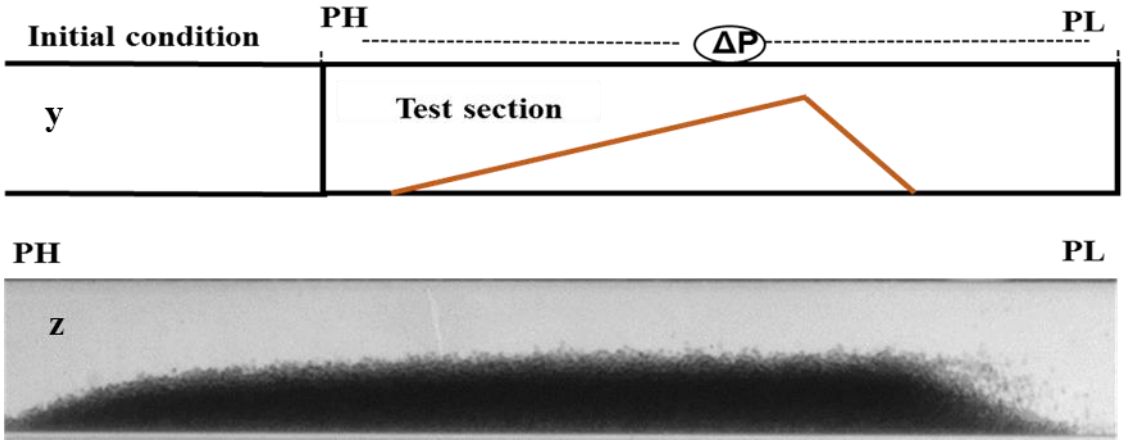

Figure 19: Pipe illustration with initial condition and test section. y)-schematic diagram showing dune is in test section and z)-real dune Figure in the test section (Section C).

In section D, Figure 16-O, pressure gradient is increasing due to Bernoulli effect because dune is at low-pressure side (PL). However, the cross-sectional area decreased due to which pressure gradient increased. Pressure gradient increased at certain point and started decreasing because now particles were washing out from the section i.e. particles were moving away from test section. We can understand better by Figure 20.1 and 20.2

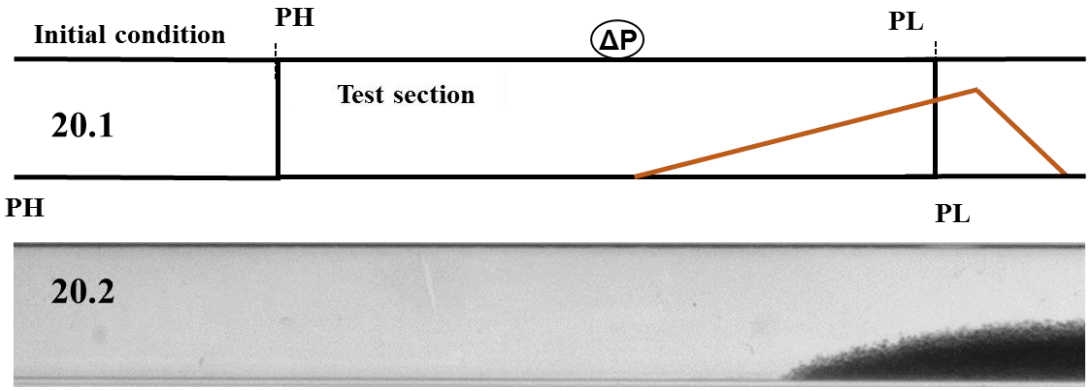

Figure 20: Pipe illustration with initial condition and test section. 20.1)-schematic diagram showing dune is at Low-pressure side and 20.2)-real dune Figure is at PL (low-pressure side) (Section D).

4.1.2.2 Analysis of bed height, length and particle velocities:

In Figure 16-r, it is obvious that the height of the bed at initial moving condition was little bit higher than the dune height in the test section. The length of the dune in test section was bit larger than length of the dune at initial moving condition. However, it was observed that the tail velocity of the dune was higher than front velocity of the dune as it can be seen apparently in Figure 21s and Figure 22t. However, in this case, the front velocity of dune was recorded about 28.98 mm/s and tail velocity of dune was around 30.92 mm/s. Comparing to previous case, the tail velocity of the dune was bit higher than front velocity. However, the dune bed was still expanding but it has less expansion because of the higher tail velocity as in Figure 16r.

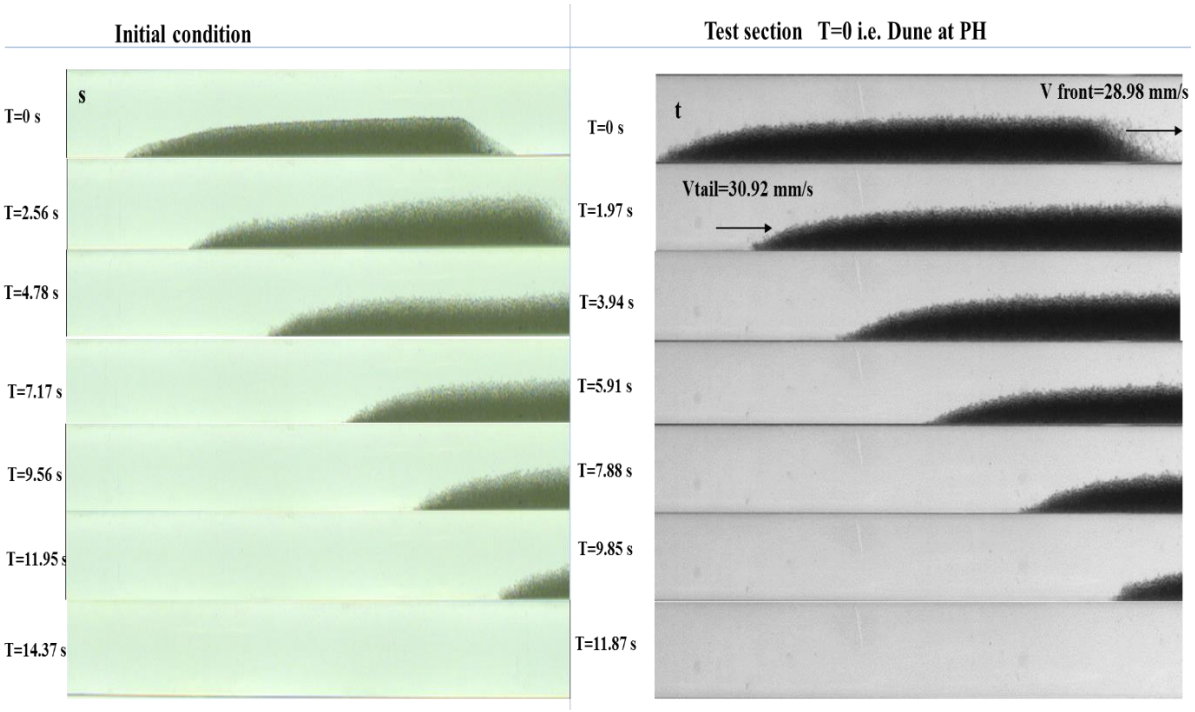

Figure 21: Real illustration of dunes. s)-Initial conditions. t)-Test section.

4.1.2.3 Key points

a) At U_{SL}=0.45 m/s, the particles were moving away from the test section faster than previous case. The bed was quite smooth with moving layer.

b) The average value of pressure gradient was higher than scenario 1 (U_{SL}=0.32 m/s). Although the behavior of the pressure gradient is similar to previous case.

c) The velocity of the dune front was less than velocity of the dune tail.

d) The height of the dune bed is decreased as dune reached to the test section and length of the dune was little bit increased in the test section than dune bed initial moving condition.

4.1.3 Scenario 3 using superficial liquid velocity (U_{SL}=0.51 m/s)

4.1.3.1 Analysis of pressure gradient as a function time

Figure 22 is the illustration of the liquid particle flow. However, x-axis comprises of time in second and y-axis consists of pressure gradient in Pa/m. However, sectioning is done for precise explanation. Anyhow, in Figure 22 section A, the pressure gradient was stable and the flow was in single phase because the dune was at initial conditions (for away from test section). In Figure 22 section B, the reduction in pressure gradient was due to Bernoulli effect and the increment in pressure gradient was because of the eddies and vortexes and turbulences of flow at dune front that caused change in pressure gradient as in Figure 18. In Figure 22 section C, we can see that the dune was now in test section and change in pressure gradient was due to frictional effect i.e. friction between wall and liquid, particles and liquid and wall and particles. After some time, the pressure gradient stayed stable and fluctuated around average value, as it can be viewed in Figure 19 for the sake of comparison. In section, D the dune was now at low-pressure side (PL) that is why the pressure gradient increased because of the Bernoulli effect and after some time it started decreasing because dune is passing away from test section as it can be seen in Figure 20. Finally, in Figure 22 section E, there was no particle in test section and flow was single phase.

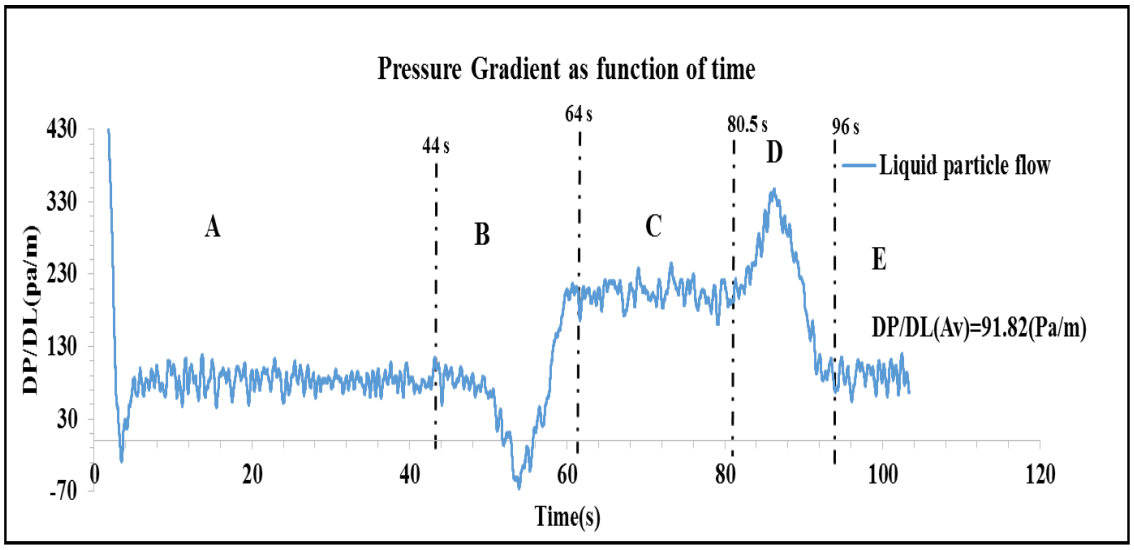

Figure 22: Results of pressure gradient as function of time with average value flow reaching to single phase

Where

DP/DL (Av) = Average Pressure gradient (Pa/m) reaching to single phase (Figure 22)

In this case, particles washed out much quicker from the test section compare to previous cases.

4.1.3.2 Analysis of bed height, length and particle velocities

Figure 23 is the combined illustration of three cases i.e. initial stationary condition, initial condition moving and test section. The x-axis comprises of length in cm and y-axis contain height in cm. It was observed that the height of the dune in test section was higher than height of dune at initial moving condition as well as initial stationary condition. Contrary to this, the length of dune in test section was comparatively less than length of dune at initial moving condition. It means that dune was more packed when it was in test section. However, the relative area and concentration of the particles in initial moving condition and test section was same but relative area was quite different in initial stationary condition. The reason behind this is that the tail velocity of the particle was much larger than front velocity so liquid inside the pipe was pushing whole dune at this (0.51 m/s) superficial liquid velocity. In addition, the flow pattern was moving bed with scouring particles. We can see in Figure 24.1 and 24.2. However, in this case, the front velocity of dune is 50.56 mm/s and tail velocity of dune was recorded around 52.53 mm/s.

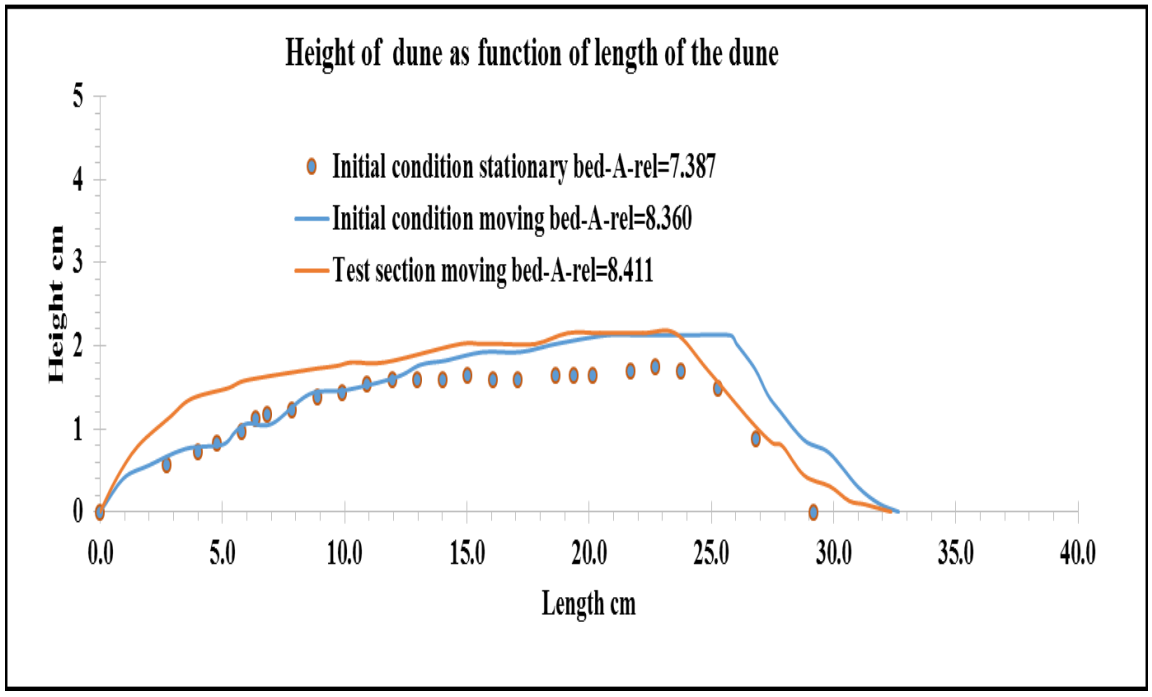

Figure 23: Height of the dune as function of length.

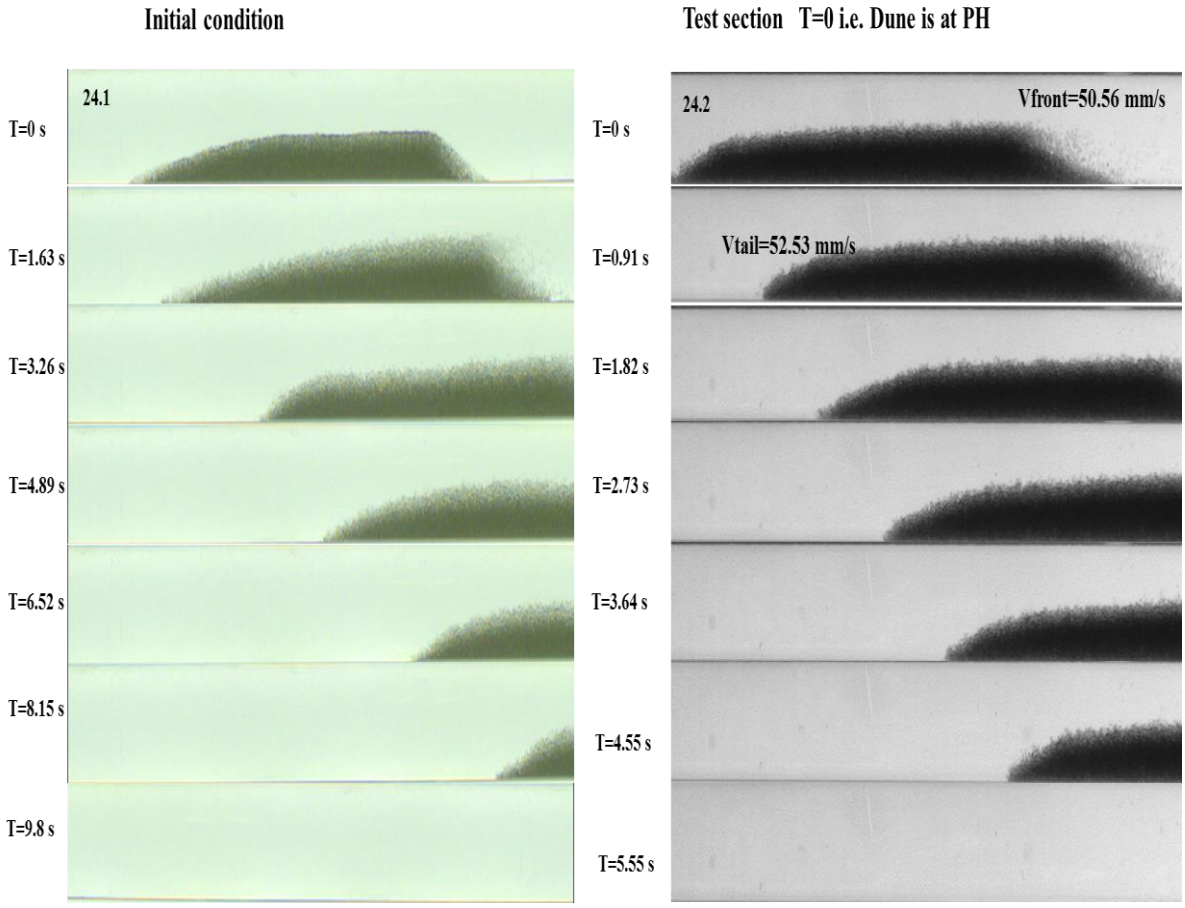

Figure 24: Real illustration of dunes. 24.1)-Initial conditions. 24.2)-Test section.

4.1.3.3 Key points

a) At U_{SL}=0.51 m/s, the particles were flushed out much faster than previous cases from the test section of horizontal pipe.

b) The average value of pressure gradient was much higher than scenario 1 (U_{SL}=0.32 m/s) and scenario 2 (U_{SL}=0.45 m/s). Although the behavior of the pressure gradient is similar to previous case.

c) The velocity of the dune front was much less than velocity of the dune tail.

d) The height of the dune increased as it reached to the test section because of higher tail velocity, the whole dune was compressed dune to which the height of the dune was increased and the length of the dune decreased.

4.1.4 Average Pressure gradient as function superficial liquid velocity (Three-Layer Model Vs Experiment)

Figure 25 indicates an average pressure gradient as function of superficial liquid velocity. However, Y-axis comprises of average pressure gradient in Pa/m (Pascal/meter) and X-axis contains superficial liquid velocity in m/s (meter/second). The average pressure gradient means the average value of pressure gradient at different superficial liquid velocities. In this Figure 25, the results from experiments and three-layer model has been compiled together to show the continuity and behavior of pressure gradient in both cases. However, the incremental trend in both cases is somehow linear. In addition, continuous increment in both cases (experiment and 3-layer model) was observed as we increased the superficial liquid velocity due to which cuttings washed out much faster from the test section so we could say that higher the pressure gradient, higher will be the cutting transport efficiency. Although, we can see the increment of pressure gradient in both cases but increment in pressure gradient in case of experiment was much higher than three-layer model. Initially in both cases, the increment was quite similar but after sometime, a sharp increase was apparent in case of experiment. Other major point is that, at lower U_{SL}, both cases were matching apparently but at higher U_{SL}, there was slight difference between experiment and three-layer model and this is because of some scoring particles that we found during experiments at high U_{SL} as in Figure 27. But in three-layer model we did not taken into consideration of effect of turbulences at dune front and some scoring particles from dune front or in other way we could say that the difference was more pronounced at higher U_{SL}. At lower flow rate, the dune bed was quite smooth and steady that is why, at lower flow rate, the experiment and three-layer model showed similar results as in Figure 26.

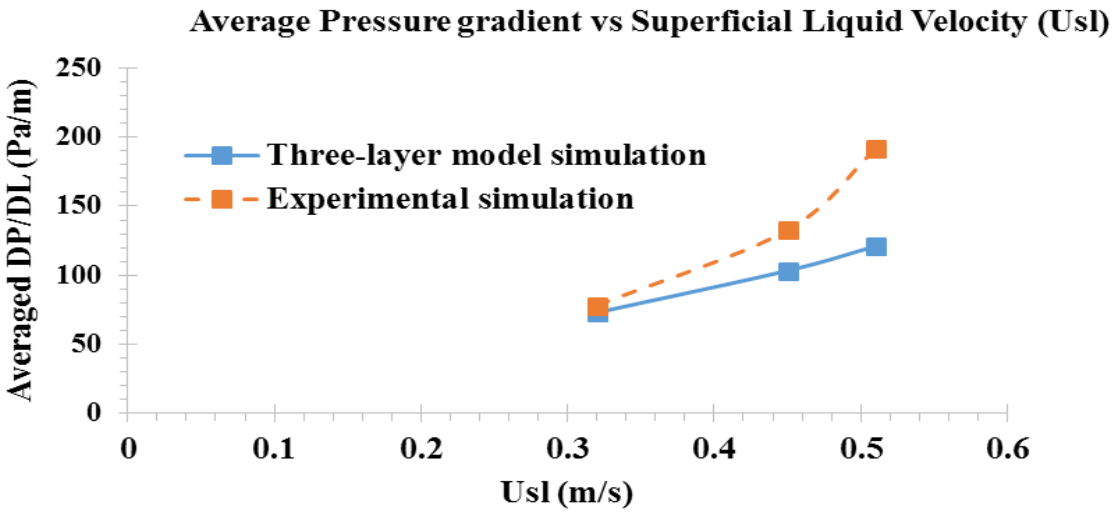

Figure 25: Averaged pressure gradient as function of superficial liquid velocity

Figure 26 and 27 are the real dune illustrations extracted during experimentations in Multiphase Lab, University of Stavanger. Figure 26 illustrates the dune bed at lower U_{SL} and Figure 27 presents the dune bed at higher U_{SL}. In Figure 26, we can see that dune bed was quite smooth with less scoring particles compare to dune bed in Figure 27, at higher U_{SL}. Although dune bed was much longer at lower U_{SL} and lower in height as compare to the dune bed at higher $U_{SL,}$ which was shorter in the length and bigger in height as in Figure 26 and 27.

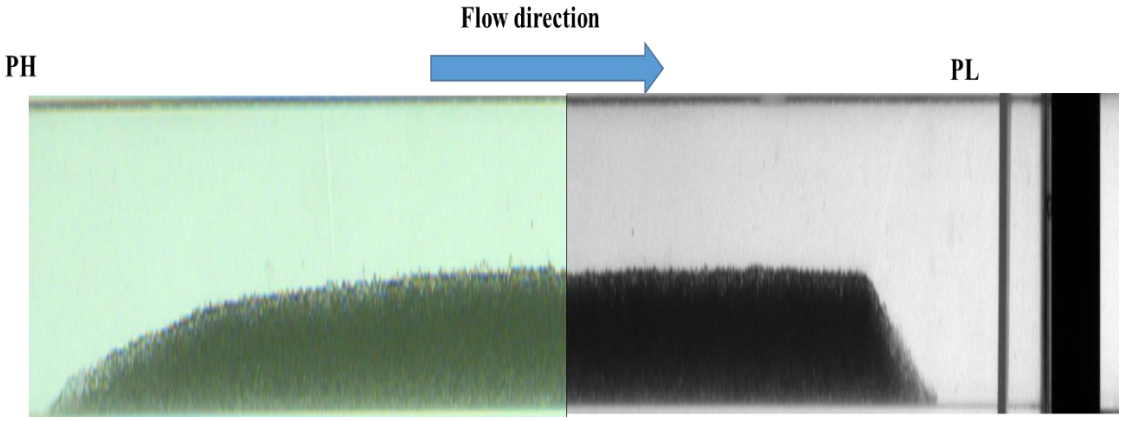

Figure 26: Dune bed illustration at lower Superficial Liquid Velocity

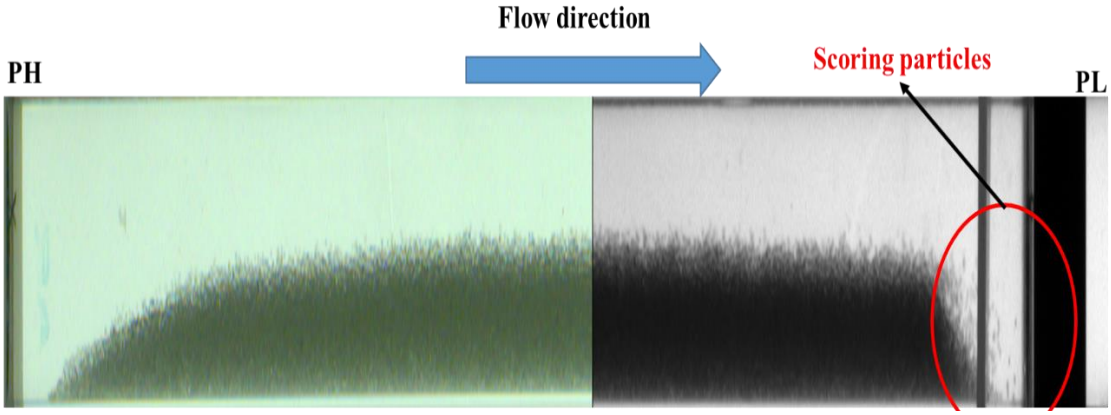

Figure 27: Dune bed illustration at higher Superficial Liquid Velocity

4.1.5 Particle travelling velocity or cutting velocity as function Superficial Liquid Velocity (U_{SL})

In Figure 28, the x-axis comprises of superficial liquid velocity (Usl) in m/s (meter/second). However, the left side of y-axis contains dune front velocity in m/s (meter/second) and right side of y-axis comprises of dune tail velocity. From Figure 28, it is obvious to say that the front and tail velocities increases apparently while increasing superficial

liquid velocity but front velocity increases at certain point and then reached to almost constant value but tail velocity is increasing continuously with the passage of time because at higher superficial liquid velocities, the tail velocities are much higher than front velocities of the dune bed. In other words, it is possible to say that whole dune is pushed by liquid from the tail side of the dune due to which dune moves much faster as we increase the superficial liquid velocity. Anyhow, it is obvious to say that at high superficial liquid velocities, the tail velocity of the dune becomes higher and front velocity of the dune becomes lower because at higher superficial liquid velocities, liquid flows faster due to which it pushes the dune bed from tail side of the dune, causing high tail velocity and lower front velocity as in Figure 28. Furthermore, Figure 29 is schematic illustration of dune bed to clarify front and tail velocity points.

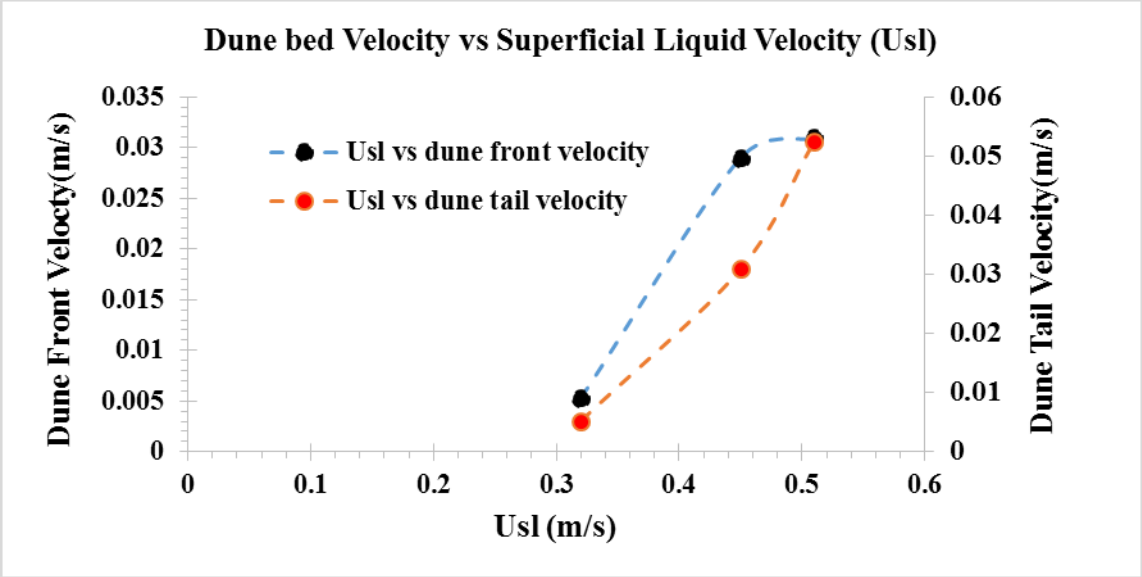

Figure 28: Liquid velocity as function of dune bed velocity

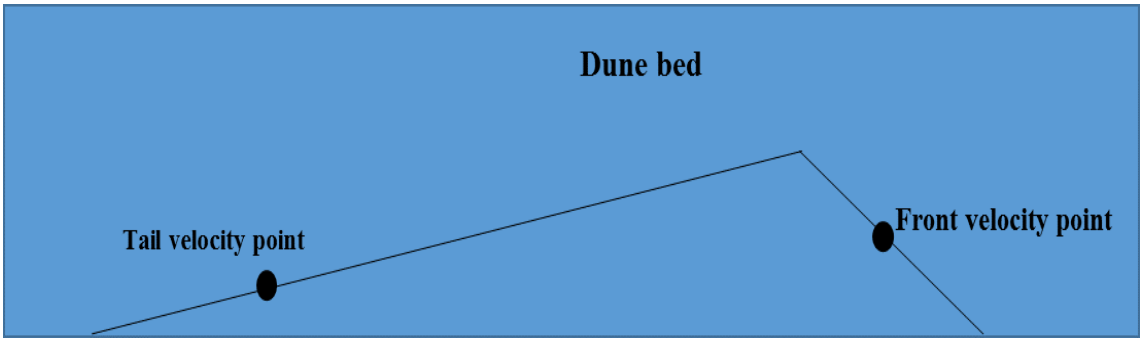

Figure 29: Schematic illustration of dune bed with front and tail velocity points

4.2 Comparison with literature

In this Table 3, we would like to express comprehensive knowledge about different scientists who worked on different topics with different parameters in the field of cutting transportation and fluid rheology. Table 4 comprises of list of title of papers with their authors.

Table 3:

<table>
<tr><th rowspan="2">Author</th><th rowspan="2">Fluid</th><th colspan="3" rowspan="2">Particle diameter</th><th colspan="2" rowspan="2">Measurement</th><th colspan="3">Minimum air fluidization velocity U_{mf} (m/s)</th></tr>
<tr><th>Sand 1</th><th>Sand 2</th><th>Sand 3</th></tr>
<tr><td rowspan="2">Felipe, C. Alberto S et al. (2004)</td><td rowspan="2">Gas</td><td>Sand 1</td><td>Sand 2</td><td>Sand 3</td><td>Inner diameter</td><td>Height of column</td><td>Sand 1</td><td>Sand 2</td><td>Sand 3</td></tr>
<tr><td>290 (µm)</td><td>470 (µm)</td><td>727 (µm)</td><td>11.12 cm</td><td>1.5 m</td><td>0.04</td><td>0.145</td><td>0.48</td></tr>
<tr><td rowspan="2">Takahashi, H., T et al. (1989)</td><td rowspan="2">Water</td><td colspan="2" rowspan="2">2.18 (mm)</td><td rowspan="2">3.06 (mm)</td><td>Inner diameter</td><td>Length of test section</td><td colspan="3" rowspan="2">-</td></tr>
<tr><td>49.7 mm</td><td>13 m</td></tr>
<tr><td rowspan="2">Prabhu Blasubramanian et al. (2005)</td><td rowspan="2">Degassed Water</td><td colspan="3" rowspan="2">-</td><td>Channel Width</td><td>Depth</td><td>Length</td><td colspan="3" rowspan="2">-</td></tr>
<tr><td>990 (µm)</td><td>207 (µm)</td><td>63.5 (mm)</td></tr>
<tr><td rowspan="2">Augusto José Garcia-Hernandez et al. (2005)</td><td rowspan="2">Water/PAC</td><td colspan="3" rowspan="2">3-5 mm</td><td>Flow loop length</td><td>Casing inner diameter.</td><td>Drill pipe outer diameter.</td><td colspan="3" rowspan="2"></td></tr>
<tr><td>(90 m)</td><td>8-inch</td><td>4.5 -inch</td></tr>
</table>

Bybee, K. (2008, February 1)	Water	-	Test section	Casing inner diameter	Outer diameter	
			100 ft long	8-inch	9-inch	

Table 3: Detail illustration of each author with different input parameters.

Table 4

Author	Title of the Journals/Papers
Felipe, C. Alberto S et al. (2004)	Time series of analysis of pressure fluctuation in Gas-Solid fluidized bed.
Takahashi, H., T et al. (1989)	Unstable flow of Sold-Liquid mixture in horizontal pipe.
Prabhu Blasubramanian et al. (2005)	Experimental study of Flow Patterns, Pressure drop, Flow Instabilities in Parallel Rectangular Minichannels.
Augusto José Garcia-Hernandez et al. (2005)	Determination of Cuttings Lag in Horizontal and Deviated Wells
Bybee, K. (2008, February 1)	Determination of Cuttings Lag in Horizontal and Deviated Wells

Table 4: Detail illustration of each author with their title.

Felipe, C. Alberto S., and S. C. S. Rocha 2004 have made study on differentiation of states of typical fluidization of gas solid bed with the help of spectrum analysis of pressure fluctuation and time series which could be useful for us to compare our results with their results in precise manners. According to their experiments and observations based on results, they found that there was periodic fluctuation in pressure with some oscillations in dune bed produced by slug flow. Although they called dune bed with piston like movement. In our case, if we would compare

with their results, we have found similarities in pressure fluctuation but behavior in our case is quite dissimilar based on scenario 1 Figure 10a, scenario 2 Figure16-O and scenario 3; Figure 22 then we will understand better that periodic fluctuation in pressure with oscillations were observed in our case but we have different behavior because of the Bernoulli Effect and some frictional impact that can cause increase or decrease in pressure variations.

Takahashi, H., T. Masuyama, and K. Noda 1989 have made investigation experimentally and theoretically on solid liquid mixture flow at lower velocities. They found that the dune velocities tend to increase as we increase the mean velocity of the mixture in the pipe flow. In our case, we have found the similarities with their observation because increase in velocities of dune bed was observed in our case while increasing superficial liquid velocity, in addition we investigated the front and tail velocity of the dune for different superficial liquid velocities as in Figure 28. Although the tail velocity of the dune bed was higher than front at higher superficial liquid velocity. Furthermore, According Takahashi, H., T. Masuyama, and K, the pressure gradient increased with solid concentration with range of maximum 10% after this range pressure gradient will start decreasing. Due this the shape of the dune bed will become more like flat than triangular but in our case, we have found the shape of the dune depends more likely on superficial liquid velocities i.e. increasing liquid velocity can cause the dune bed to become more flatter and fasters irrespective of the concentration of the solid particles. In addition, in our case, the change in pressure gradient with the passage of time was dependent on Bernoulli Effect and some frictional forces, which causes the pressure gradient to increase or decrease in pressure fluctuation behavior.

Prabhu Blasubramanian and Satish G. Kandlikar (2005) have performed experimental study on flow patterns, pressure drop and flow instabilities in rectangular minichannels. They have found increased in pressure drop with increase in surface temperature. Although according to them, the pressure drop remains constant for given mass flux. Pressure drop follows the periodic trend of fluctuation with small changes. In our case of single phase Figure 10b, we used water as flowing media; there was periodic fluctuations in pressure drop, which remain constant with passage of time at constant mass flow rate, which is quite similar to their investigation of pressure drop. However, when it comes to two phase or liquid particle flow, we have found quite similar periodic fluctuation but with different behavior and at different stages as it can be seen in scenario 1 Figure 10a, scenario 2-Figure 16-O and scenario 3, Figure 22 because of the Bernoulli and frictional effect in the horizontal pipe flow. Therefore, our results are quite dissimilar when it comes to solid liquid flow in pipe.

Augusto José Garcia-Hernandez 2005 did experiments on horizontal and slightly inclined section of the wellbore to determine the cutting lag. In addition, he also worked on solid liquid flow pattern, particle slip velocity and particle tracking. He used water as fluid with cutting size of 3-5 mm. They found that the cutting velocity increases with increase in liquid velocity of flow rate but this increasing trend is not linear. Although we have found same behavior in our observation of determining particle velocity by increasing flow rate. We use different superficial liquid velocities and an increase in particle velocity were investigated apparently in our results. In short, an increase in particle velocity was experienced with increase in superficial liquid velocity as in Figure 28.

Bybee, K. (2008, February 1) performed experimental study on cutting lag or slip velocity. He presented a graph in his paper and title of the graph is "Cutting velocity in moving layer vs liquid velocity". He observed the increased in cutting velocity while increasing liquid velocity in horizontal section as well as 20 degree from horizontal section. Anyhow, the increment follows the linear trend. We observed same behavior in our observation of determining particle velocity by increasing superficial liquid velocities. We use different superficial liquid velocities and an increase in particle velocity was apparently observed in our results as it can be seen in Figure 28.

4.3 Comparison with three-layer model

We would like to present comparison of three-layer model simulation with experimental results of liquid-particle flow in horizontal section of the pipe. The 3-layer model work was done by Milad Khatibi (PhD candidate (University of Stavanger) and Johnny Petersen (IRIS Stavanger). However, same initial and boundary conditions for both cases (Experiment and three-layer model) were used. The simulation from three-layer model is same with experiment because we considered same bed height conditions and distance from high-pressure side is similar. Furthermore, the three-layer dynamic model was initiated for superficial liquid velocity (Usl) 0.45 m/s. We would like to illustrate the real measurements that we used for three-layer dynamic model as well and for experiments. It can be seen more precisely in Figure 30:

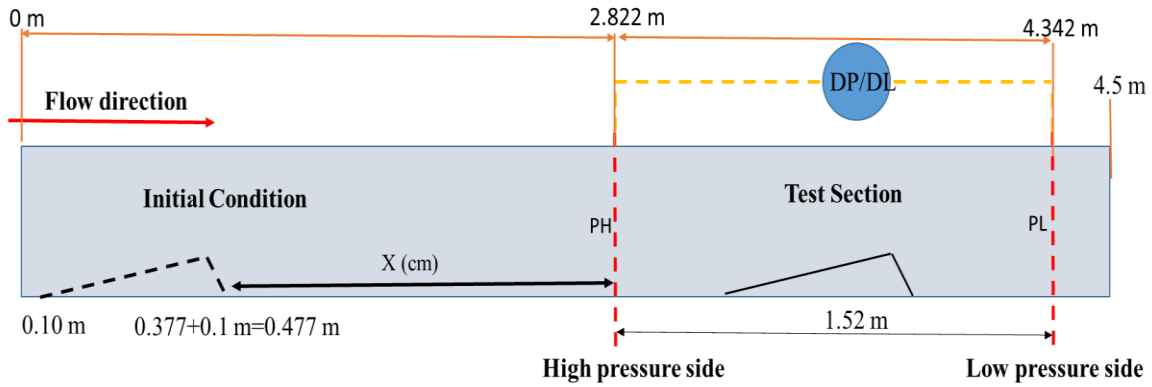

Figure 30: Schematic illustration with measurements with initial and boundary conditions (Medium scale flow loop, horizontal section).

4.3.1 Comparing 3-layer dynamic model with experiment using U_{SL}= 0.45 m/s

The Figure 31 indicates the pressure gradient as function of time. However, the X-axis comprises of time in seconds and Y-axis contains pressure gradient in Pascal/meter (Pa/m). In this graph, we compared the experimental results with two cases of three-layer dynamic model. However, liquid-particle flow precisely observed under superficial liquid velocity of 0.45 m/s. In addition, we used friction factor FF = 0.13 and FF = 0.10 in 3-layer dynamic model to see how friction effect the pressure gradient. Although, the length of the dune is higher in this case and the whole dune is moving much faster towards the test section. From graph, it is quite apparent that both (experimental and both cases of three-layer model) having same behavior. Initially in both cases, flow is in single phase because the dune was at initial condition and we were not recording pressure gradient either at this point. However, with the passage of time, the pressure gradient

reduced in both cases because of the Bernoulli effect. Although, the Bernoulli effect has to do with area above dune, which reduces when liquid flowing together with particles form a dune bed. When dune reaches to high-pressure side (pressure transducer mounted), the area above dune reduces so the pressure gradient reduces as well. Although, the decrement is quite sharp in case of experiment. However, in case of three-layer model result, the decrement in pressure gradient is not sharp and quite smooth as compared to experimental result. After some time, the pressure gradient increases in both cases because of the frictional effects due to particle-particle interaction and particle-wall interaction and some vortexes that can cause increase in pressure gradient in both cases. After sometime, the pressure gradient is stable and have periodic fluctuation for some time in both cases because dune bed is moving inside the test section, there are some turbulences of flow at the dune front and frictional effects due to particle-particle interaction and particle-wall interaction. With the passage of time, pressure gradient increased dramatically in all cases because of the Bernoulli effect. Although we have effect of friction and turbulence but Bernoulli effect more pronounced here. Finally, the dune is at low-pressure side so pressure gradient increased when dune hit the boundary of low-pressure side. Finally, the pressure gradient has started decreasing in both cases because particles were moving away from the test section but in case of experiment the decrement is quite sharp as compared to three-layer model and eventually the pressure gradient is stable in all cases because no particle was flowing together with water in the test section.

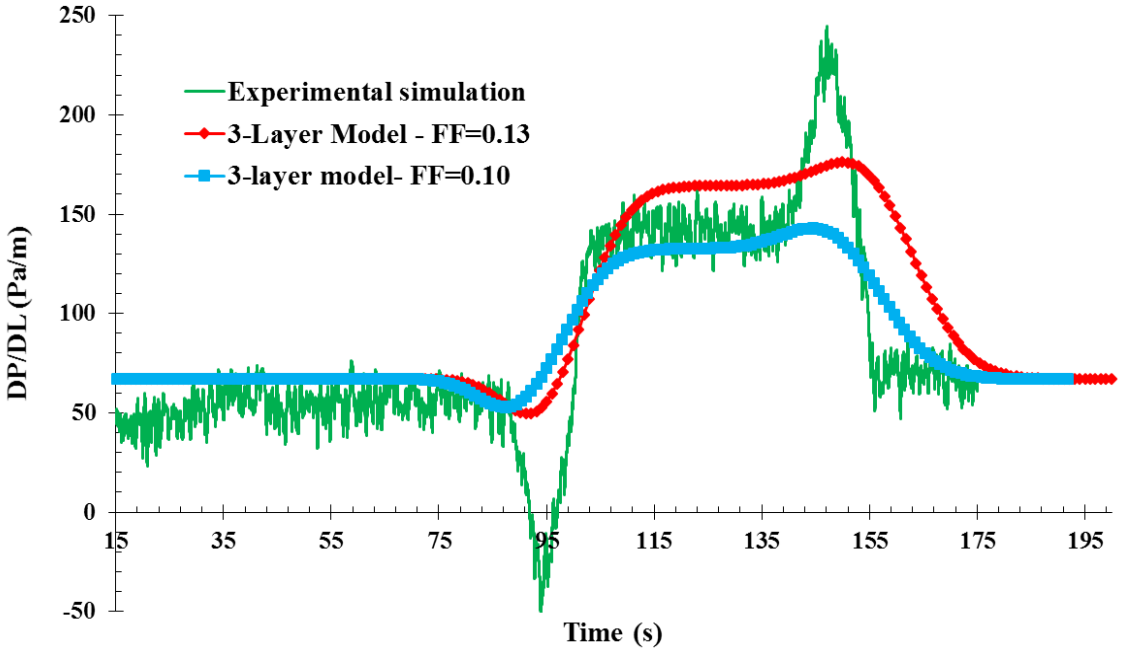

Figure 31: Comparison of three-layer dynamic model simulation with experiment using USL= 0.45 m/s

4.3.1.1 Use of two different friction factors in 3-layer model FF= 0.10 and FF = 0.13

In addition, we used two different friction factors to see how pressure gradient will behave when we increase the friction factor into the 3-layer model. From Figure 31, An increase in pressure gradient was observed while increasing friction in 3-layer dynamic model. Although, frictional pressure drop in both cases (FF= 0.10 and FF = 0.13) is quite apparent. At FF (Friction factor) = 0.10, the pressure gradient is somehow showing an agreement with experiment but when we increased the friction factor (FF= 0.13) then pressure gradient increased much compare to FF=0.10 and went over the experimental simulation but still matching with experiment. To summarize, it is possible to say that higher the friction higher will be the pressure gradient as per Darcy friction factor correlation:

$$\frac{\Delta p}{L} = f_{\mathrm{D}} \cdot \frac{\rho}{2} \cdot \frac{\langle v \rangle^2}{D}, \qquad \text{eq 36}$$

ΔP = Pressure (Pa/m)

ρ = density (kg/m^3)

v = velocity (m/s)

L= Length (m)

f_D = Darcy friction factor

D = Inner diameter of the pipe (m)

4.3.1.2 Précised justification of less increment and decrement in pressure gradient in both cases (Friction factor = 0.10 and Friction factor 0.13) of 3-layer model

In Figure 31, we can see that the decrement in pressure gradient is high in case of experiment compare to 3-layer model where the pressure gradient decreased comparatively less. Because in case of 3-layer model, when dune reached at PH (high-pressure side) it is much longer in length this is because of the dune front velocity which was higher in this case. The area above dune reduced but the reduction in area above dune was less (area above dune was higher) because of the wider distributions of the particles in 3-layer model compare to experiment where the area above dune also reduced but the reduction was quite higher in case of experiment. It could explain better by eq 37 and condition 1.

4.3.1.3 Case 1 (PH= changing, PL= constant) dune is at PH

Dune bed is on PH (high-pressure side) and in both cases, area above dune decreases so PH reduced (PL is constant) due to which pressure gradient decreases as well based on eq 37. However, the decrement in pressure gradient is less in case of 3-layer model because area above dune in case of 3-layer model was higher (because of the wider distributions of the particle) than area above dune in case of experiment. As we can see Figure 32:

$$A_{3-layer} > A_{Experiment} \quad \text{(Condition 1)}$$

$A_{3-layer}$ = Area above dune in case of 3-layer model

$A_{Experiment}$ = Area above dune in case of experiment

$$\Delta p = P_H - P_L \quad \text{(eq 37)}$$

P_H = High-pressure side of the test section (changing)

P_L = Low-pressure side of the test section (constant)

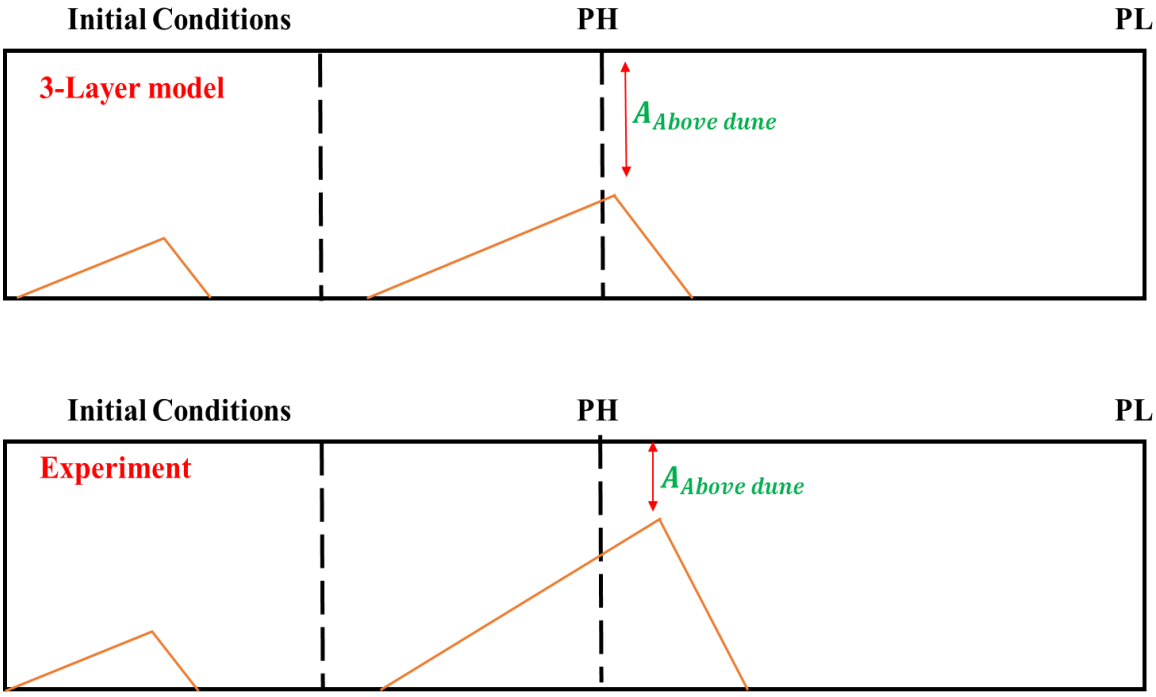

Figure 32: Schematic illustration of dune bed in case of 3-layer model and experiment at initial condition and at PH.

4.3.1.4 Case 2 (PH= constant, PL= changing) dune is at PL

In this case, dune bed is now at PL (low-pressure side) so area above dune decreases due to which PL decreases, (PH is constant) eventually pressure gradient increases based on eq 37. However, the increment in pressure gradient is less in case of 3-layer model and this is

because of the area above dune, which is higher compare to area in case of experiment. We can see eq 37 and condition 1 for clarification. However, Figure 33 indicates that dune which is at PL (low pressure side of the test section).

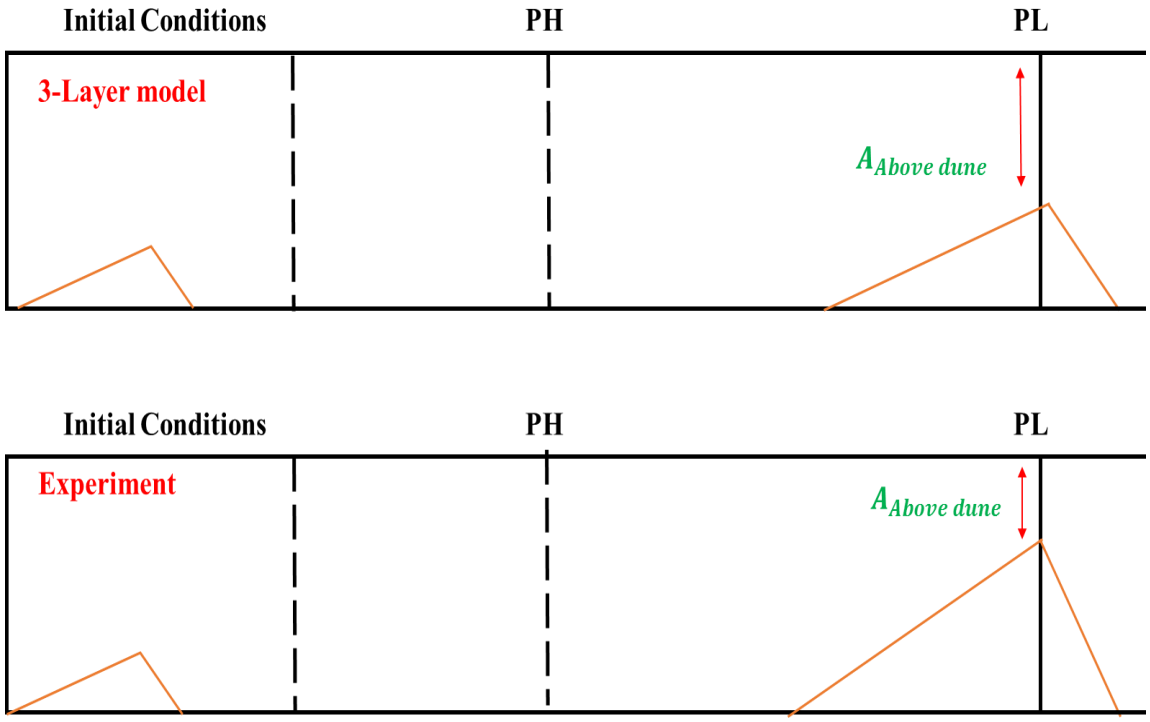

Figure 33: Schematic illustration of dune bed in case of 3-layer model and experiment at initial condition and at PL.

5 Conclusions

Single phase and liquid particle flow experiments were performed to compare different aspects. In single-phase flow, we used flowing water in horizontal section of the pipe, during this time we recorded the pressure drop and flow rate. We used different superficial liquid velocities to investigate further, how liquid velocity would affect the cutting transportation. However, we used glass spherical particles in liquid-particle flow experiments. Furthermore, pressure drop was measured for different superficial liquid velocities. The images of dune bed was acquired by using high speed camera and the velocities of dune front and tail computed using MATLAB application to see how fast particles were moving with liquid flow. Although, the height of the dune bed was determined to investigate the increase or decrease in height of the dune bed while increasing superficial liquid velocities. In addition, the comparison of our study has done with literature to see the similarities and differences so far. Furthermore, we compared our results with three-layer dynamic model as well to see if the simulations and experimental results show an agreement or observing a different phenomenon.

1) During experimentations, a smooth dune bed was founded at lower superficial liquid velocities. Because of lower tail velocities and higher front velocities of the dune bed, a longer dune bed was experienced with apparently lower height.

2) At high superficial liquid velocities, the dune bed was not smooth and the height was changing at every section of the pipe. Although, the dune bed was shorter in the length because whole dune bed was compressed from tail side of the dune bed because of higher tail velocities.

3) The average pressure gradient increases as we increase the superficial liquid velocity. However, the incremental trend is somehow linear in this case as it can be seen in Figure 25. Although, a slight difference is experienced in experiment and three-layer model result, which is more pronounced at higher superficial liquid velocities. From literature, the same behavior of pressure gradient is observed, which acknowledges that pressure gradient increases as we increase Usl.

4) From Figure 28, it is quite apparent that the front velocity of the dune increases up to the certain point but after that, the value became quite stable. However, the dune tail velocity is increasing continuously as we increase the superficial liquid velocity. The reason is that at higher superficial liquid velocities, the dune front velocity is

less than dune tail velocity. The whole dune is compressed because of the higher tail velocity and lower dune front velocity.

5) From literature, an increase in cutting or particles travelling velocity was experienced while increasing superficial liquid velocity, which shows an agreement with our case, from Figure 28, we found that cutting velocity increases as we increase the Usl. In addition, periodic fluctuations in pressure analysis were observed, which is quite similar with our results but the behavior of pressure gradient is different with the literature. In our case, Bernoulli, frictional and turbulence effects are more pronounce but in literature, the pressure gradient is quite stable with period fluctuation in pressure.

6) After combining the results of three-layer dynamic model and experiment, we found that both have same behavior (Bernoulli, frictional and turbulence effects) but the amplitude of the increment or decrement in case of three-layer model is comparatively smaller as compared to experiment.

6 Recommendations for future work

1) Use of non-Newtonian fluid such as PAC (Poly anionic cellulose) is recommended to analyze the rheological behavior of the fluid more precisely.
2) CFD (Computational Fluid Dynamic) modeling is highly recommended to compare the experimental results to see the similarities and differences so far.
3) A small modification is needed in the injection system of medium scale flow loop to let the particles comes out easily from hydro-cyclone.
4) Use of different concentration of the particles could be interesting to see the effect of particle concentration on the pressure gradient.

7 References

Bizanti, M. S., & Alkafeef, S. F. (2003, January 1). A Simplified Hole Cleaning Solution to Deviated and Horizontal Wells. Society of Petroleum Engineers. doi:10.2118/81412-MS

Company, M. S. (2004). MI-PAC*R Poly anionic cellulose is fluid loss and Viscosity control additive. Houston Textas: MI SWACO A Schlumberger Company. Retrieved from www.miswaco.com

Crowe, C. T., Schwarzkopf, J. D., Sommerfeld, M., & Tsuji, Y. (2011). Multiphase flows with Droplets and Particles. CRC Press Taylorand Francis Group.

Egenti, N. B. (2014, August 5). Understanding Drill-cuttings Transportation in Deviated and Horizontal Wells. Society of Petroleum Engineers. doi:10.2118/172835-MS

Khatibi, M., Potokin, N., & Time, R. W. (2016). Experimental investigation of Effects of salts on rhelogical properties of non-Newtonian Fluids University of Helsinki, Finland.

Kiijarvi, J. (2011). Darcy friction factor formulae in turbulent pipe flow. Lunowa Fluid Mechanics Paper, 110727.

Bizanti, M. S. (1983). Fluid dynamics of well-bore bottom-hole cleaning (Doctoral dissertation).

Mohammadsalehi, M., & Malekzadeh, N. (2011, January 1). Optimization of Hole Cleaning and Cutting Removal in Vertical, Deviated and Horizontal Wells. Society of Petroleum Engineers. doi:10.2118/143675-MS

Neutrium. (2012). Pressure loss in Pipe. *Pressure loss in Pipe*. Retrieved from https://neutrium.net/fluid_flow/pressure-loss-in-pipe/

PELLUTEL POLY-ANIONIC-CELLULOSE. (n.d.). Retrieved from SHANDONG YITENG NEW MATERIAL CO.LTD: http://www.yitengchem.cn/en/index.php?c=content&a=list&catid=181

Shook, C. A., & Roco, M. C. (1991). Slurry Flow, Principle and Practice, pub.

Walker, S., & Li, J. (2000, January 1). The Effects of Particle Size, Fluid Rheology, and Pipe Eccentricity on Cuttings Transport. Society of Petroleum Engineers. doi:10.2118/60755-MS

Su, Ze, and J. S. Gudmundsson. "Friction factor of perforation roughness in pipes." SPE Annual Technical Conference and Exhibition. Society of Petroleum Engineers, 1993

Raffel, M., Willert, C. E., Wereley, S., & Kompenhans, J. (2013). Particle image velocimetry: a practical guide. Springer.

http://www.dantecdynamics.com/measurement-principles-of-piv

Adrian, Ronald J., and Jerry Westerweel. *Particle image velocimetry*. No. 30. Cambridge University Press, 2011.

Doron, P., and D. Barnea. "A three-layer model for solid-liquid flow in horizontal pipes." International Journal of Multiphase Flow 19.6 (1993): 1029-1043.

Woo, N. S., Kim, Y. J., Kwon, J. K., Chung, S. K., & Park, E. S. (2011, January). A study on the solid-liquid rotating flow for cuttings transportation in inclined annulus. In The Twenty-first International Offshore and Polar Engineering Conference. International Society of Offshore and Polar Engineers.

Goharzadeh, A., Rodgers, P., & Wang, L. (2013). Experimental Characterization of Slug Flow on Solid Particle Transport in a 1 Deg Upward Inclined Pipeline. *Journal of Fluids Engineering*, *135*(8), 081304.

Peysson, Y. (2004). Solid/liquid dispersions in drilling and production. Oil & gas science and technology, 59(1), 11-21.

Bilgesu, H. I., Ali, M. W., Aminian, K., & Ameri, S. (2002, January 1). Computational Fluid Dynamics (CFD) as a Tool to Study Cutting Transport in Wellbores. Society of Petroleum Engineers. doi:10.2118/78716-MS

Parsi, M., Vieira, R. E., Agrawal, M., Srinivasan, V., McLaury, B. S., Shirazi, S. A., … Hampel, U. (2015, September 4). Computational Fluid Dynamics (CFD) Simulation of Multiphase Flow and Validating Using Wire Mesh Sensor. BHR Group.

Felipe, C. Alberto S., and S. C. S. Rocha. "Time series analysis of pressure fluctuation in gas-solid fluidized beds." Brazilian Journal of Chemical Engineering 21.3 (2004): 497-507.

Takahashi, H., T. Masuyama, and K. Noda. "Unstable flow of a solid-liquid mixture in a horizontal pipe." International Journal of Multiphase Flow 15.5 (1989): 831-841.

Balasubramanian, Prabhu, and Satish G. Kandlikar. "Experimental study of flow patterns, pressure drop, and flow instabilities in parallel rectangular minichannels." Heat Transfer Engineering 26.3 (2005): 20-27.

Augusto José Garcia-Hernandez, “Determination of Cuttings Lag in Horizontal and Deviated Wells” University of Tulsa, Drilling Research Projects, B.S. in Mechanical Engineering, Central University of Venezuela. This report is prepared for TUDRP Advisory Board Meeting, November 14th-15th, 2005, Tulsa-Oklahoma.

Bybee, K. (2008, February 1). Determination of Cuttings Lag in Horizontal and Deviated Wells. Society of Petroleum Engineers. doi:10.2118/0208-0056-JPT

8 Appendix

8.1 Attachment 1

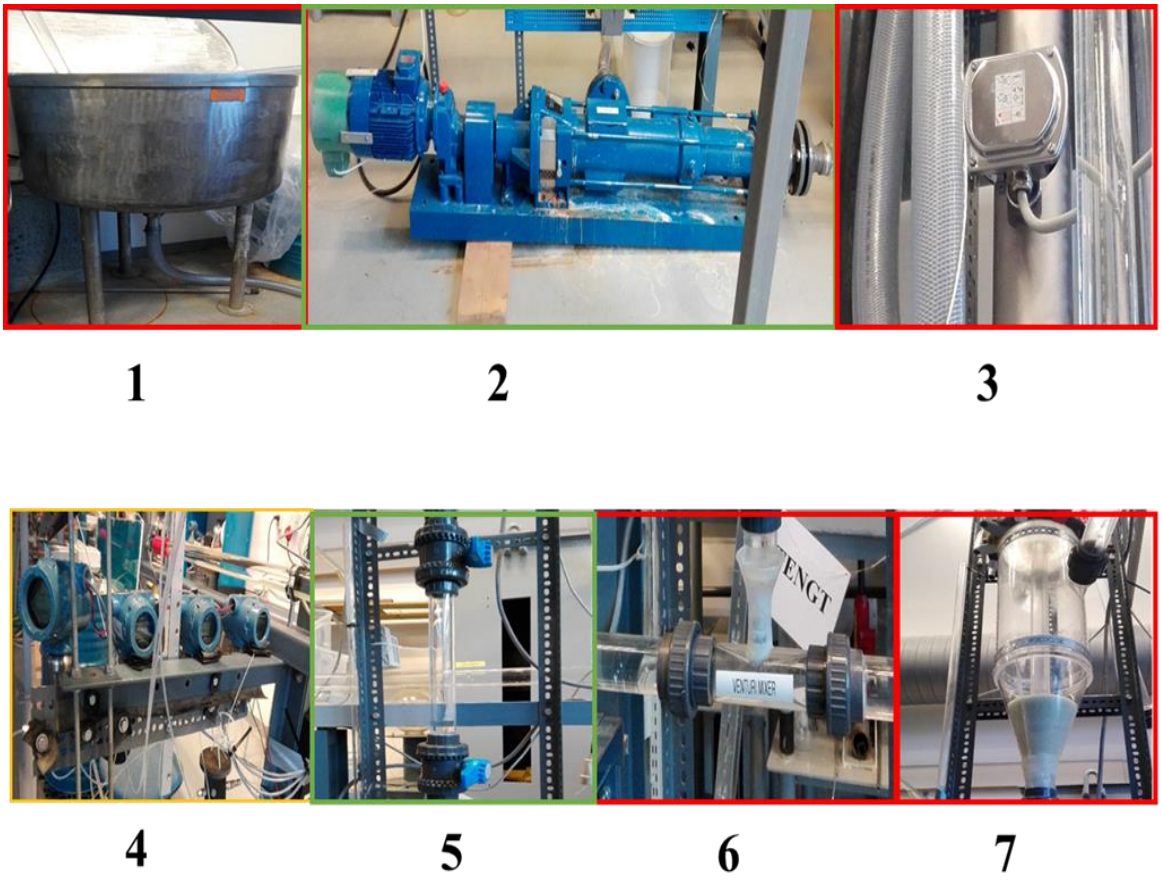

Figure 34: Real illustration of equipments used in Multiphase Laboratory University of Stavanger

1. **Tank/ Liquid container:**

This is real picture of the tank (liquid container). Although we use tap water to fill container for making experiments and in this tank, we have small strainer to avoid the particles to settle down in the tank that may eventually interrupt the performance of the pump.

2. **Pump:**

Screw gauge pump that we use in multiphase lab to pump the liquid from container to the medium scale flow loop.

3. **Flow meter:**

Coriolis flow meter is used to measure the real flow rate through the LabVIEW software in the computer in Kg/hr.

4. **Pressure transducer:**

   Pressure transducers or pressure sensor are connected to each side of section to measure the pressure drop at high-pressure side as well as low-pressure side. However, it is very crucial to remove the bubbles from small pipes (which connects the pressure sensor to each side of the section)

5. **Particle Injection system:**

Two valves just below the hydro cyclone are use to control the particle injection from the hydro cyclone to the medium scale flow loop. While particle injection we should be careful and we should not open both valves at same time that may affect the accuracy of the results.

6. **Venturi:**

   Venturi mixer is use to enhance the speed of injection of the particles into the medium scale flow loop.

7. **Hydro cyclone:**

This is the particle injection and collection setup. We inject the particle through hydro cyclone into the medium scale flow loop. When the particle passed out every section of the pipeline then finally collected into the hydro cyclone particles due to high density settle down into hydro-cyclone and water goes into the tank again.

8.2 Attachment 2

MATLAB code

```
clc
clear
close all;
RESULTS1_black = [];


%% offset for pressure gadient (DP)

DP_h_0 = -0.4913;   % horizontal
DP_5_0 = 0.1158;   %5 degree inclination from horizontal
DP_35_0 = -8.6847 ;  %35 degree
DP_bend_0 = -1.2935 ; % bend %it is horionztal


%% Constant values

d = 40/1000;                              %pipe diameter m
d2 = 25/1000;                              % inner pipe diameter m  % Drill
string
L_H = 1.52;          %unit m               %Distance between two tap pressure
L_5 = 1.52;          %unit m               %Distance between two tap pressure
L_35 = 0.60;         %unit m               %Distance between two tap pressure
L_bend = 0.57;       %unit m               %Distance between two tap pressure

%% reading the text file
%row number of the first data in the text
S1=2;

% Reading excel file (from Data Acquisition)
% Text name
filename1= 'Testf7.txt';
file=fopen(filename1);
NUM1= textscan(file,'%s %s %s %s %s %s');
fclose(file);

% converting the array to matrix
for i=1:6
val1(:,i) = str2double(NUM1{1,i});

end

%row number of the last data in the text files
E1=size(val1,1);


%generating the time frequency is 250  delta_t=1/250 sec
for i=1:E1
val_time(i,1) = i/250 ;
end



% Computing variables (Mass Flow rate, Temp, Usl_pipe, Usl_annulus_5 degree,
Dp-H, Dp-5 degree,
% Dp-35 degree, Dp-Bend (90 degree)

mfr_1 = mean(val1(S1:E1,5))/3600;         %unit (kg/s)
Temp_1 = mean(val1(S1:E1,6));          %unit (kg/m^3)
Usl_1 = mfr_1/(998*pi()*d^2/4);               %unit (m/s)
Usl_5_1 = mfr_1/(998*pi()*(d^2-d2^2)/4);              %unit (m/s)
DP_h_1 = (mean(val1(S1:E1,1)) /L_H)-DP_h_0;       %unit (mbar/m)
DP_5_1 = (mean(val1(S1:E1,3))/L_5)-DP_5_0;        %unit (mbar/m)
DP_35_1 = (mean(val1(S1:E1,2)) /L_35)-DP_35_0;       %unit (mbar/m)
```

```
DP_bend_1 = (mean(val1(S1:E1,4)) /L_bend)-DP_bend_0;     %unit (mbar/m)

% Min and Max
DP_hmin_1(S1:E1,1) = (min(val1(S1:E1,1)) /L_H)-DP_h_0;      %unit (mbar/m)
DP_hmax_1(S1:E1,1) = (max(val1(S1:E1,1)) /L_H)-DP_h_0;      %unit (mbar/m)
DP_5min_1(S1:E1,1) = (min(val1(S1:E1,3))/L_5)-DP_5_0;       %unit (mbar/m)
DP_5max_1(S1:E1,1) = (max(val1(S1:E1,3))/L_5)-DP_5_0;       %unit (mbar/m)
DP_35min_1(S1:E1,1) = (min(val1(S1:E1,2)) /L_35)-DP_35_0;      %unit
(mbar/m)
DP_35max_1(S1:E1,1) = (max(val1(S1:E1,2)) /L_35)-DP_35_0;      %unit
(mbar/m)
DP_bendmin_1(S1:E1,1) = (min(val1(S1:E1,4)) /L_bend)-DP_bend_0;     %unit
(mbar/m)
DP_bendmax_1(S1:E1,1) = (max(val1(S1:E1,4)) /L_bend)-DP_bend_0;     %unit
(mbar/m)



%LowPass Fillter
val1_mfr = smooth(val1(S1:E1,5));
val1_Temp = smooth(val1(S1:E1,6));
val1_DP_h = (smooth(val1(S1:E1,1))/L_H)-DP_h_0;
val1_DP_5 = (smooth(val1(S1:E1,3))/L_5)-DP_5_0;
val1_DP_35 = (smooth(val1(S1:E1,2))/L_35)-DP_35_0;
val1_DP_bend = (smooth(val1(S1:E1,4))/L_bend)-DP_bend_0;

% Plot
Figure;
s(1) = subplot(2,2,1);
s(2) = subplot(2,2,2);
s(3) = subplot(2,2,3);
s(4) = subplot(2,2,4);

%Horizontal section
plot(s(1),val_time(S1:E1,1),val1_DP_h,'k',val_time(S1:E1,1),DP_hmin_1(S1:E1,
1),'r:',val_time(S1:E1,1),DP_hmax_1(S1:E1,1),'r:');
title(s(1),strcat('Pressure gradient - Horizontal', ' Usl=
',num2str(Usl_1),' [m/s]'));
xlabel(s(1),'Time [s]','FontSize',14);
ylabel(s(1),'DP/Dl [mbar/m]','FontSize',14);


RESULTS1_black = [mfr_1, Temp_1, Usl_1,Usl_5_1,
DP_h_1,DP_5_1,DP_35_1,DP_bend_1]
```